Seventh International Conference on Computational Fluid Dynamics (ICCFD7), Big Island, Hawaii, July 9-13, 2012

ICCFD7-3601

Very-high-order conservative discretization of diffusive terms with variable viscosity

G.A. Gerolymos* and I. Vallet*
Corresponding author: georges.gerolymos@upmc.fr

* Université Pierre-et-Marie-Curie, 4 place Jussieu, 75005 Paris, France.

Abstract: We study very-high-order conservative discretizations for diffusive terms with variable viscosity, which are present in the compressible Navier-Stokes equations, based on the construction of numerical viscous fluxes at cell-interfaces. We introduce a novel conservative approach for the discretization of $\big(v(x)\,u'(x)\big)'$ which yields $O(\Delta x^{2s})$ accuracy on the stencil $\{i-s,\cdots,i,\cdots,i+s\}$, thus obtaining the same order-of-accuracy as nonconservative methods on the same stencil, and improving upon previous conservative proposals which are $O(\Delta x^{2\lceil\frac{s}{2}\rceil})$-accurate on the same stencil. The extension of the scheme to 2-D and 3-D regular Cartesian grids, including cross-derivatives, is described. Several typical 1-D and 3-D computational examples substantiate the order-of-accuracy of the method.

Keywords: High-Order Schemes, Reconstruction, Viscous Terms, Diffusion Equation, Compressible Navier-Stokes Equations.

1 Introduction

Very-high-order accuracy is essential in several practical applications where the solution contains widely varying spatial and temporal scales, as in the case of direct numerical simulation (DNS) of compressible turbulent flows in physical space [1, 2, 3, 4, 5, 6, 7, 8]. Since such flows may contain shockwaves [1, 4, 6, 7], particular care is taken in designing and using very-high-order conservative methods for the convective part of the equations, WENO schemes [9] being a widely adopted choice [4, 5, 6, 7, 8]. On the other hand the discretization of the diffusive (viscous) terms has received less attention. Many authors revert to a nonconservative formulation [3], the compact scheme developed by Lele [10] being a popular choice [11], while others prefer using low-order conservative schemes for the viscous terms [8], combined with very-high-order schemes for the convective terms [12].

However, nonconservative approaches do not warrant global equilibrium of forces in the momentum equation [13], which is only achieved approximately, with accuracy depending on the truncation error of the scheme on the grid used in the particular computation. Therefore, when very coarse grids are used, as *eg* in the case of preliminary ill-resolved DNS calculations, the error in global equilibrium may be not negligible.[1] It is precisely such global equilibrium relations that conservation ensures [13].

Zingg et al. [14] have developed a conservative scheme for the viscous terms on the stencil $\mathrm{S}_{i,3,3}:=\{i-3,\cdots,i+3\}$, which yields an $O(\Delta x^4)$-accurate approximation of $\big(v(x)\,u'(x)\big)'$. As will be shown in the present work the formulation of Zingg et al. [14] can be easily extended to the general stencil $\mathrm{S}_{i,s,s}:=\{i-s,\cdots,i+s\}$ to yield $O(\Delta x^{2\lceil\frac{s}{2}\rceil})$-accurate numerical approximation of $\big(v(x)\,u'(x)\big)'$. Notice that the order-of-accuracy obtained for the viscous terms is lower than the accuracy $O(\Delta x^{(2s-1)})$ obtained by the WENO$(2s-1)$ schemes for the convective terms on the same stencil [15, 16, 8]. Shen et al. [17], working on the same $\mathrm{S}_{i,3,3}$ stencil as Zingg et al. [14], developed an alternative $O(\Delta x^4)$-accurate conservative formulation, which they showed to have smaller truncation error (but the same order-of-accuracy).

[1] *eg* in fully-developed incompressible plane channel flow [8] the global equilibrium relation is $2\bar{\tau}_w+L_y\partial_x\bar{p}=0$, where $\bar{\tau}_w$ is the wall-shear-stress $\partial_x\bar{p}$ is the streamwise pressure-gradient, and L_y is the channel's height

Both these conservative approaches [14, 17] construct fluxes[2] at the cell-interfaces using a face-based (and face-centered) stencil. Alternatively, Gassner et al. [18], extending the generalized Riemann problem [19] to diffusive terms, proposed a cell-based reconstruction, leading to left (L) and right (R) reconstructing polynomials on the 2 sides of each face, which are combined through a diffusion Riemann solver [18], to construct the interface flux for the diffusive terms. In the present work, we concentrate on the face-based approach. Furthermore, we assume that the investigated problems are sufficiently smooth, postponing the treatment of weak solutions (*eg* through WENO reconstruction [9, 20]) to a future specific study. Throughout the paper we work on general stencils parametrized by the order-parameter s, so that all of the developed relations and results are scalable to arbitrary order-of-accuracy.

2 Fluxes for $\Big(v(x)u'(x)\Big)'$

Both Zingg et al. [14] and Shen et al. [17] developed their schemes on the stencil $\mathrm{S}_{i,3,3} := \{i-3, \cdots, i+3\}$. Shen et al. [17] express explicitly the numerical fluxes $[\check{F}_{(vu'),\mathrm{SZC},\mathrm{S}_{i,2,3}}]_{i+\frac{1}{2}}$ and $[\check{F}_{(vu'),\mathrm{SZC},\mathrm{S}_{i-1,2,3}}]_{i-\frac{1}{2}}$, defined on the stencils $\mathrm{S}_{i,2,3} := \{i-2, \cdots, i+3\}$ and $\mathrm{S}_{i-1,2,3} = \mathrm{S}_{i,3,2} := \{i-3, \cdots, i+2\}$, respectively, which yield an $O(\Delta x^4)$-accurate approximation of $(vu')'_i$. On the other hand, Zingg et al. [14] gave directly the finite-difference expression approximating $(vu')'_i$ to $O(\Delta x^4)$, on the stencil $\mathrm{S}_{i,3,3} := \{i-3, \cdots, i+3\}$. Their method can easily be interpreted in terms of interface-fluxes, using reconstruction concepts [21]. In the following we show how both these schemes can be extended to arbitrary $O(\Delta x^{2\lceil \frac{s}{2} \rceil})$ order-of-accuracy on the general centered (around i) stencil $\mathrm{S}_{i,s,s} := \{i-s, \cdots, i+s\}$. Then, we present a more compact approach yielding an asymptotically twice more accurate $O(\Delta x^{2s})$ approximation of $(vu')'_i$ on $\mathrm{S}_{i,s,s} := \{i-s, \cdots, i+s\}$.

The explanation of the scheme of Zingg et al. [14] is more intricate than the original finite-differencing analysis, in order to bring forward intermediate steps and stencils (Fig. 1), where accuracy is lost. This more intricate analysis, also applied to the scheme of Shen et al. [17], highlights the reasons of loss of accuracy and provides guidance towards improvement.

2.1 Definitions

The following tools of polynomial reconstruction [22, 9, 21] are used, both to describe and extend to arbitrary order-of-accuracy the methods of Zingg et al. [14] and of Shen et al. [17], and to develop the present approach. On a homogeneous 1-D grid

$$x_i = x_1 + (i-1)\Delta x \qquad \Delta x = \mathrm{const} \in \mathbb{R}_{>0} \tag{1a}$$

we define the stencil

$$\mathrm{S}_{i,M_-,M_+} := \{i - M_-, \cdots, i + M_+\} \qquad ; \qquad M := M_- + M_+ \geq 0 \tag{1b}$$

of $M+1$ points in the neighbourhood of i, with M_- neighbours to the left and M_+ neighbours to the right. Assume that the real function $f : \mathbb{R} \longrightarrow \mathbb{R}$ is sufficiently smooth, and that there exists a real function $h : \mathbb{R} \longrightarrow \mathbb{R}$ whose sliding (with x) cell-averages are equal to $f(x)$, *ie*

$$f(x) = \frac{1}{\Delta x} \int_{x-\frac{1}{2}\Delta x}^{x+\frac{1}{2}\Delta x} h(\zeta) d\zeta \quad \forall x \in [a,b] \overset{[21,\ (9)]}{\Longrightarrow} f'(x) = \frac{h(x+\frac{1}{2}\Delta x) - h(x-\frac{1}{2}\Delta x)}{\Delta x} \quad \forall x \in [a,b] \tag{1c}$$

Because of (1c), an approximation to $h(x)$ can serve to define interface fluxes at $i \pm \frac{1}{2}$ for the approximation of $f'(x)$. It simplifies notation to write, for 2 functions $f : \mathbb{R} \to \mathbb{R}$ and $h : \mathbb{R} \to \mathbb{R}$ satisfying (1c)

$$(1c) \iff h = R_{(1;\Delta x)}(f) \tag{1d}$$

[2] although the original scheme of Zingg et al. [14] gave the expression for the numerical approximation of $\Big(v(x)u'(x)\Big)'$, it can be easily reinterpreted in terms of interface fluxes (§2.2)

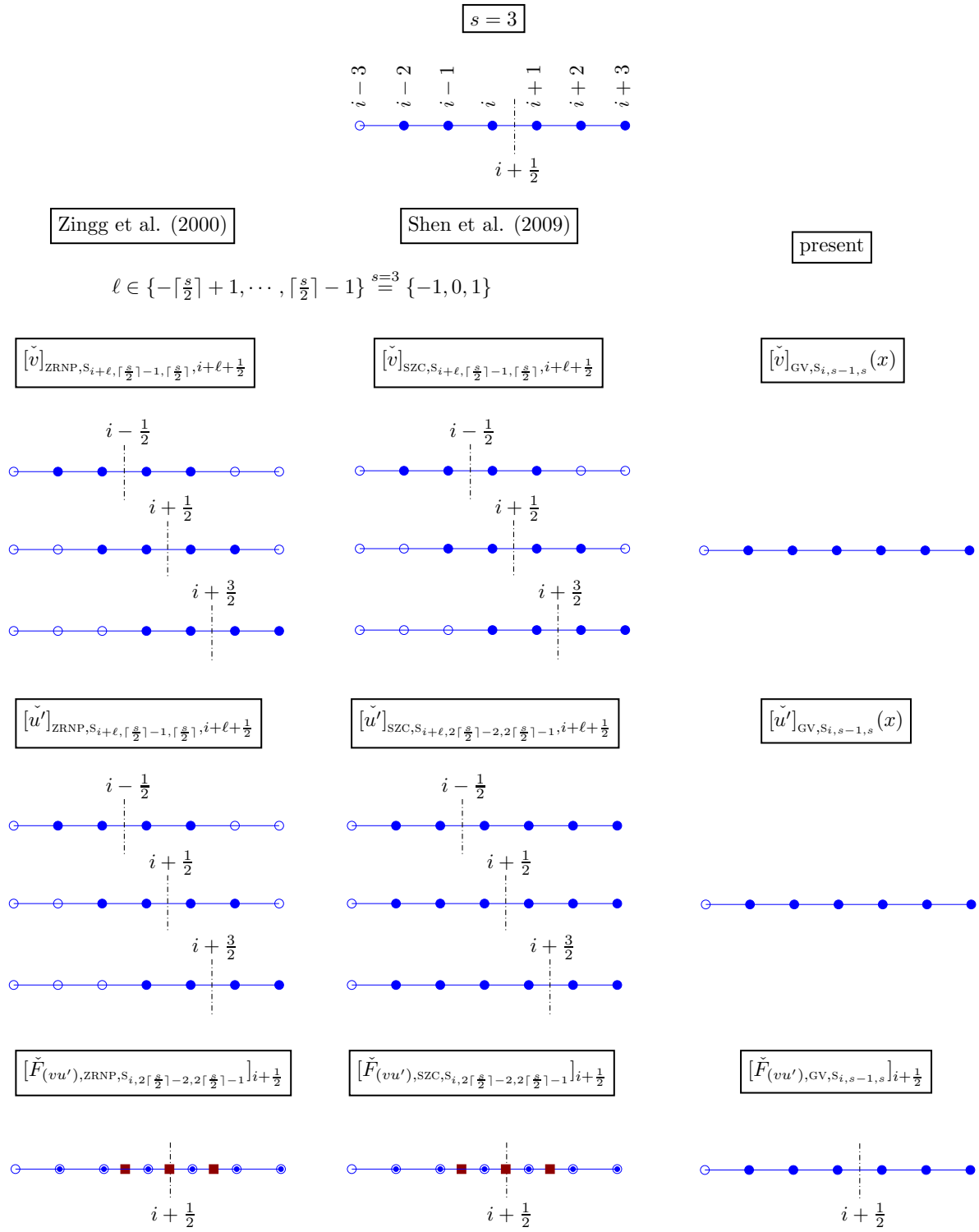

Figure 1: Example for $k = 2 \implies s_{\lceil \frac{s}{2} \rceil = 2} = 3$ of the different approximation steps and stencils used for the construction of the numerical fluxes at $i + \frac{1}{2}$ for the approximation of $[(vu')']_i$, on the stencil $\mathrm{S}_{i,s,s} := \{i - s, \cdots, i + s\} \overset{s=3}{=} \{i - 3, \cdots, i + 3\}$, $[\check{F}_{(vu'),\mathrm{ZRNP},\mathrm{S}_{i,2\lceil \frac{s}{2} \rceil - 2,2\lceil \frac{s}{2} \rceil - 1}}]_{i+\frac{1}{2}}$ (2f) of Zingg et al. [14] (§2.2) and $[\check{F}_{(vu'),\mathrm{SZC},\mathrm{S}_{i,2\lceil \frac{s}{2} \rceil - 2,2\lceil \frac{s}{2} \rceil - 1}}]_{i+\frac{1}{2}}$ (3f) of Shen et al. [17] (§2.3), both of which use intermediate values at the interfaces $i + \ell + \frac{1}{2}$ ($\ell \in \{-\lceil \frac{s}{2} \rceil + 1, \cdots, \lceil \frac{s}{2} \rceil - 1\} \overset{s=3}{=} \{-1, 0, +1\}$), and $[\check{F}_{(vu'),\mathrm{GV},\mathrm{S}_{i,s-1,s}}]_{i+\frac{1}{2}}$ (6) developed in the present work (§2.4), which uses reconstruction of interpolating polynomials on the entire stencil ($\cdot - \cdot - \cdot$ interface where a quantity is approximated, $\circ$ not used, $\bullet$ point used for the computation at the interface, $\blacksquare$ intermediate values at interfaces computed using $\odot$ points).

and we will call f and h a reconstruction pair in view of the computation of the 1-derivative [21].

We will note

$$p_{I,M_-,M_+}(x_i+\xi\Delta x;x_i,\Delta x;f) \overset{[21,\ (45e)]}{=} \sum_{\ell=-M_-}^{M_+} \alpha_{I,M_-,M_+,\ell}(\xi)\ f(x_i+\ell\Delta x) \tag{1e}$$

$$\overset{[21,\ (51b)]}{=} f(x_i+\xi\Delta x)+O(\Delta x^{M+1}) \tag{1f}$$

the Lagrange interpolating polynomial on $\mathrm{S}_{i,M_-,M_+} := \{i-M_-,\cdots,i+M_+\}$, of degree $M := M_- + M_+$, which approximates $f(x)$ to $O(\Delta x^{M+1})$, and whose derivative with respect to x,

$$p'_{I,M_-,M_+}(x_i+\xi\Delta x;x_i,\Delta x;f) := [\frac{d}{dx}p_{I,M_-,M_+}](x;x_i,\Delta x;f) \overset{(1e)}{=} \frac{1}{\Delta x}\sum_{\ell=-M_-}^{M_+} \alpha'_{I,M_-,M_+,\ell}(\xi)\ f(x_i+\ell\Delta x) \tag{1g}$$

$$\overset{(1f)}{=} f'(x_i+\xi\Delta x)+O(\Delta x^{M}) \tag{1h}$$

approximates $f'(x)$ to $O(\Delta x^M)$. The corresponding Lagrange reconstructing polynomial is defined by requiring that

$$p_{I,M_-,M_+}(x;x_i,\Delta x;f) = \frac{1}{\Delta x}\int_{x-\frac{1}{2}\Delta x}^{x+\frac{1}{2}\Delta x} p_{R_1,M_-,M_+}(x;x_i,\Delta x;f)d\zeta \quad \forall x\in\mathbb{R} \tag{1i}$$

This polynomial, which is also of degree M [21, Lemma 3.1, p. 277], can be represented by

$$p_{R_1,M_-,M_+}(x_i+\xi\Delta x;x_i,\Delta x;f) \overset{[21,\ (45d)]}{=} \sum_{\ell=-M_-}^{M_+} \alpha_{R_1,M_-,M_+,\ell}(\xi)\ f(x_i+\ell\Delta x) \tag{1j}$$

$$\overset{[21,\ (51a)]}{=} h(x_i+\xi\Delta x)+O(\Delta x^{M+1}) \tag{1k}$$

and approximates, to $O(\Delta x^{M+1})$ [21, Proposition 4.7, p. 292], the function $h(x)$, whose sliding (with x) cell-averages are equal to $f(x)$. The Lagrange reconstructing polynomial (1j) defines interface fluxes for the computation of $f'(x)$ to $O(\Delta x^{M+1})$ [21]. By analogy with (1c), we have [21, Corollary 4.9, p. 295]

$$f'(x_i)+O(\Delta x^{M+1}) \overset{[21,\ (60)]}{=} \frac{p_{R_1,M_-,M_+}(x_i+\frac{1}{2}\Delta x;x_i,\Delta x;f)-p_{R_1,M_-,M_+}(x_i-\frac{1}{2}\Delta x;x_{i-1},\Delta x;f)}{\Delta x} \tag{1l}$$

$$= \frac{p_{R_1,M_-,M_+}(x_i+\frac{1}{2}\Delta x;x_i,\Delta x;f)-p_{R_1,M_-+1,M_+-1}(x_i-\frac{1}{2}\Delta x;x_i,\Delta x;f)}{\Delta x} \tag{1m}$$

By (1j), the reconstructing polynomials at $i+\frac{1}{2}$ and $i-\frac{1}{2}$, calculated on the stencils $\mathrm{S}_{i,M_-,M_+} := \{i-M_-,\cdots,i+M_+\}$ and $\mathrm{S}_{i-1,M_-,M_+} := \{i-1-M_-,\cdots,i-1+M_+\} =: \mathrm{S}_{i,M_-+1,M_+-1}$, respectively, define the interface fluxes for calculating $f'_i := f'(x_i)$ to $O(\Delta x^{M_-+M_++1}) = O(\Delta x^{M+1})$. The fundamental functions of Lagrange reconstruction $\alpha_{R_1,M_-,M_+,\ell}\in\mathbb{R}_M[\xi]$ are polynomials of degree M which can be explicitly calculated from the analytical expressions [23] of the fundamental functions of Lagrange interpolation $\alpha_{I,M_-,M_+,\ell}\in\mathbb{R}_M[\xi]$. Analytical expressions for $\alpha_{R_1,M_-,M_+,\ell}(\xi)$ were obtained by Shu [22, (2.19), p. 336], and can also be expressed using the elements of the inverse of the Vandermonde matrix [21, (45g), p. 287]. These analytical expressions [24, (10,11,14), p. 2768] are easily implemented using symbolic calculus [25] and will be used to explicitly evaluate and tabulate the coefficients of the different schemes.[3]

[3] In [21, pp. 301–303] it was shown that numerical fluxes for the approximation of the 2-derivative $f''(x)$ can be constructed by applying twice the reconstruction operator (1d). However, the case of the numerical approximation of $(vu')'$, which is studied here, is more complicated.

2.2 Zingg et al. [14]

Both the scheme of Zingg et al. [14] extended to arbitrary order-of-accuracy here, and the scheme of Shen et al. [17] studied below (§2.3), are defined on stencils with an odd number of neighbours on each side of point i, $\mathrm{S}_{i,2k-1,2k-1} := \{i-2k+1,\cdots,i+2k-1\}$ $(k\in\mathbb{N}_{>0})$, on which they are $O(\Delta x^{2k})$-accurate. For the purpose of comparison with the present method we describe them on the general centered (around i) stencil $\mathrm{S}_{i,s,s} := \{i-s,\cdots,i+s\}$ $(s\in\mathbb{N}_{>0})$, by replacing $k := \lceil\frac{s}{2}\rceil$, *ie* on the stencil $\mathrm{S}_{i,2\lceil\frac{s}{2}\rceil-1,2\lceil\frac{s}{2}\rceil-1} := \{i-2\lceil\frac{s}{2}\rceil+1,\cdots,i+2\lceil\frac{s}{2}\rceil-1\}$ $(s\in\mathbb{N}_{>0})$, where they are $O(\Delta x^{2\lceil\frac{s}{2}\rceil})$-accurate. When $s=2k-1$ $(k\in\mathbb{N}_{>0})$, the entire stencil $\mathrm{S}_{i,s,s} := \{i-s,\cdots,i+s\}$ $(s\in\mathbb{N}_{>0})$ is used, as in the present scheme (§2.4), whereas when $s=2k$ $(k\in\mathbb{N}_{>0})$ the schemes of Zingg et al. [14] and of Shen et al. [17] do not use the end-points $\{i-s,i+s\}$. Although Zingg et al. [14] followed a standard finite-differencing approach in developing their scheme on $\mathrm{S}_{i,3,3} := \{i-3,\cdots,i+3\}$, we describe the method in the following in terms of equivalent polynomial interpolations, both because this allows the explicit analytical calculation of all scheme-coefficients in a straightforward manner, but also because it clarifies order-of-accuracy relations by (1g, 1l), and the more detailed results in [21].

Interpreted in terms of interface fluxes

$$\begin{aligned}[(vu')'_i]_{\mathrm{ZRNP},\mathrm{S}_{i,2\lceil\frac{s}{2}\rceil-1,2\lceil\frac{s}{2}\rceil-1}} =& \frac{[\check{F}_{(vu'),\mathrm{ZRNP},\mathrm{S}_{i,2\lceil\frac{s}{2}\rceil-2,2\lceil\frac{s}{2}\rceil-1}}]_{i+\frac{1}{2}} - [\check{F}_{(vu'),\mathrm{ZRNP},\mathrm{S}_{i-1,2\lceil\frac{s}{2}\rceil-2,2\lceil\frac{s}{2}\rceil-1}}]_{i-\frac{1}{2}}}{\Delta x}\\ =&[(vu')'](x_i) + O(\Delta x^{2\lceil\frac{s}{2}\rceil}) \end{aligned} \tag{2a}$$

the method of Zingg et al. [14] computes the numerical flux $[\check{F}_{(vu'),\mathrm{ZRNP},\mathrm{S}_{i,2\lceil\frac{s}{2}\rceil-2,2\lceil\frac{s}{2}\rceil-1}}]_{i+\frac{1}{2}}$ on the stencil $\mathrm{S}_{i,2\lceil\frac{s}{2}\rceil-2,2\lceil\frac{s}{2}\rceil-1} := \{i-2\lceil\frac{s}{2}\rceil+2,\cdots,i+2\lceil\frac{s}{2}\rceil-1\}$ (Fig. 1). First, $O(\Delta x^{2\lceil\frac{s}{2}\rceil})$-accurate interpolations of $v(x)$ and $u(x)$ at the cell-interfaces $\mathrm{S}_{i+\frac{1}{2},\lceil\frac{s}{2}\rceil-1,\lceil\frac{s}{2}\rceil-1} := \{i-\lceil\frac{s}{2}\rceil+\frac{3}{2},\cdots,i+\lceil\frac{s}{2}\rceil-\frac{1}{2}\}$ are constructed. The interpolation at each cell-interface $i+\ell+\frac{1}{2}$ $(\ell\in\{-\lceil\frac{s}{2}\rceil+1,\cdots,\lceil\frac{s}{2}\rceil-1\}$ is obtained on the stencil $\mathrm{S}_{i+\ell,\lceil\frac{s}{2}\rceil-1,\lceil\frac{s}{2}\rceil} := \{i+\ell-\lceil\frac{s}{2}\rceil+1,\cdots,i+\ell+\lceil\frac{s}{2}\rceil\}$ which is centered around $i+\ell+\frac{1}{2}$.

$$\begin{aligned}[\check{v}]_{\mathrm{ZRNP},\mathrm{S}_{i+\ell,\lceil\frac{s}{2}\rceil-1,\lceil\frac{s}{2}\rceil},i+\ell+\frac{1}{2}} :=& p_{I,\lceil\frac{s}{2}\rceil-1,\lceil\frac{s}{2}\rceil}(x_{i+\ell}+\tfrac{1}{2}\Delta x; x_{i+\ell},\Delta x; v)\\ \overset{(1e)}{=}& \sum_{p=-\lceil\frac{s}{2}\rceil+1}^{s} \alpha_{I,\lceil\frac{s}{2}\rceil-1,\lceil\frac{s}{2}\rceil,p}(\tfrac{1}{2})\; v_{i+\ell+p} \quad \overset{(1f)}{=} v(x_{i+\ell+\frac{1}{2}}) + O(\Delta x^{2\lceil\frac{s}{2}\rceil}) \end{aligned} \tag{2b}$$

$$\begin{aligned}[\check{u'}]_{\mathrm{ZRNP},\mathrm{S}_{i+\ell,\lceil\frac{s}{2}\rceil-1,\lceil\frac{s}{2}\rceil},i+\ell+\frac{1}{2}} :=& p'_{I,\lceil\frac{s}{2}\rceil-1,\lceil\frac{s}{2}\rceil}(x_{i+\ell}+\tfrac{1}{2}\Delta x; x_{i+\ell},\Delta x; u)\\ \overset{(1g)}{=}& \frac{1}{\Delta x}\sum_{q=-\lceil\frac{s}{2}\rceil+1}^{\lceil\frac{s}{2}\rceil} \alpha'_{I,\lceil\frac{s}{2}\rceil-1,\lceil\frac{s}{2}\rceil,q}(\tfrac{1}{2})\; u_{i+\ell+q} \overset{(1h)}{=} u'(x_{i+\ell+\frac{1}{2}}) + O(\Delta x^{2\lceil\frac{s}{2}\rceil}) \end{aligned} \tag{2c}$$

By (1f) we know that the interpolation on $\{i+\ell-\lceil\frac{s}{2}\rceil+1,\cdots,i+\ell+\lceil\frac{s}{2}\rceil\}$ is $O(\Delta x^{2\lceil\frac{s}{2}\rceil})$. The derivative of the interpolating polynomial in (2c) is an $O(\Delta x^{2\lceil\frac{s}{2}\rceil-1})$-accurate approximation of the derivative in general, but is $O(\Delta x^{2\lceil\frac{s}{2}\rceil})$ at $i+\ell+\frac{1}{2}$ because the stencil $\mathrm{S}_{i+\ell,\lceil\frac{s}{2}\rceil-1,\lceil\frac{s}{2}\rceil} := \{i+\ell-\lceil\frac{s}{2}\rceil+1,\cdots,i+\ell+\lceil\frac{s}{2}\rceil\}$ is centered around $i+\ell+\frac{1}{2}$ (a linear interpolation between 2 points yields an $O(\Delta x^2)$-accurate approximation of the derivative at the center of the interval but only $O(\Delta x)$ elsewhere). Then we use the $O(\Delta x^{2\lceil\frac{s}{2}\rceil})$-accurate approximations to $vu'(x)$ at the $2\lceil\frac{s}{2}\rceil-1$ points $i+\ell+\frac{1}{2}$ $(\ell\in\{-\lceil\frac{s}{2}\rceil+1,\cdots,\lceil\frac{s}{2}\rceil-1\}$ to obtain an $O(\Delta x^{2\lceil\frac{s}{2}\rceil})$-accurate reconstruction of the function $[R_{(1;\Delta x)}(vu')](x)$,[4] whose sliding with x cell-averages (1c, 1d) are equal to $v(x)u'(x)$. For ease of notation we define as $[\check{vu'}]_{\mathrm{ZRNP},\mathrm{S}_{i,2\lceil\frac{s}{2}\rceil-2,2\lceil\frac{s}{2}\rceil-1}}(x)$ the Lagrange interpolating

[4] in (1c) $v(x)u'(x)$ is $f(x)$ and the unknown function $[R_{(1;\Delta x)}(vu')](x)$ is $h(x)$

polynomial defined by the $2\lceil\frac{s}{2}\rceil-1$ values $[\check{v}]_{\text{ZRNP},\text{S}_{i+\ell,\lceil\frac{s}{2}\rceil-1,\lceil\frac{s}{2}\rceil},i+\ell+\frac{1}{2}}[\check{u'}]_{\text{ZRNP},\text{S}_{i+\ell,\lceil\frac{s}{2}\rceil-1,\lceil\frac{s}{2}\rceil},i+\ell+\frac{1}{2}}$,

$$
\begin{aligned}
[\check{vu'}]_{\text{ZRNP},\text{S}_{i,2\lceil\frac{s}{2}\rceil-2,2\lceil\frac{s}{2}\rceil-1}}(x) &\overset{\text{(1e)}}{:=} \sum_{\ell=-\lceil\frac{s}{2}\rceil+1}^{\lceil\frac{s}{2}\rceil-1} \Bigg(\alpha_{I,\lceil\frac{s}{2}\rceil-1,\lceil\frac{s}{2}\rceil-1,\ell}\Big(\frac{x-x_{i+\frac{1}{2}}}{\Delta x}\Big) \\
&\qquad \Big([\check{v}]_{\text{ZRNP},\text{S}_{i+\ell,\lceil\frac{s}{2}\rceil-1,\lceil\frac{s}{2}\rceil},i+\ell+\frac{1}{2}}[\check{u'}]_{\text{ZRNP},\text{S}_{i+\ell,\lceil\frac{s}{2}\rceil-1,\lceil\frac{s}{2}\rceil},i+\ell+\frac{1}{2}}\Big)\Bigg) \\
&\overset{\text{(1f, 2b, 2c)}}{=} v(x)u'(x) + O(\Delta x^{2\lceil\frac{s}{2}\rceil}) \qquad \text{(2d)}
\end{aligned}
$$

although only the halfpoint-values (2b, 2c) appear in the final scheme.[5] The interface-flux is obtained by the reconstruction of $[\check{vu'}]_{\text{ZRNP},\text{S}_{i,2\lceil\frac{s}{2}\rceil-2,2\lceil\frac{s}{2}\rceil-1}}(x)$ (2d) on the stencil $\text{S}_{i+\frac{1}{2},\lceil\frac{s}{2}\rceil-1,\lceil\frac{s}{2}\rceil-1} := \{i+\frac{3}{2}-\lceil\frac{s}{2}\rceil,\cdots,i-\frac{1}{2}+\lceil\frac{s}{2}\rceil\}$ which is centered around $i+\ell+\frac{1}{2}$

$$
\begin{aligned}
&[\check{F}_{(vu'),\text{ZRNP},\text{S}_{i,2\lceil\frac{s}{2}\rceil-2,2\lceil\frac{s}{2}\rceil-1}}]_{i+\frac{1}{2}} := p_{R_1,\lceil\frac{s}{2}\rceil-1,\lceil\frac{s}{2}\rceil-1}(x_{i+\frac{1}{2}};x_{i+\frac{1}{2}},\Delta x;[\check{vu'}]_{\text{ZRNP},\text{S}_{i+\ell,2\lceil\frac{s}{2}\rceil-2,2\lceil\frac{s}{2}\rceil-1}}) \\
&= \sum_{\ell=-\lceil\frac{s}{2}\rceil+1}^{\lceil\frac{s}{2}\rceil-1} \Big(\alpha_{R_1,\lceil\frac{s}{2}\rceil-1,\lceil\frac{s}{2}\rceil-1,\ell}(0)\ \Big([\check{v}]_{\text{ZRNP},\text{S}_{i+\ell,\lceil\frac{s}{2}\rceil-1,\lceil\frac{s}{2}\rceil},i+\ell+\frac{1}{2}}[\check{u'}]_{\text{ZRNP},\text{S}_{i+\ell,\lceil\frac{s}{2}\rceil-1,\lceil\frac{s}{2}\rceil},i+\ell+\frac{1}{2}}\Big)\Big) \\
&\qquad = [R_{(1;\Delta x)}(vu')](x_{i+\frac{1}{2}}) + O(\Delta x^{2\lceil\frac{s}{2}\rceil}) \qquad \text{(2e)}
\end{aligned}
$$

Again, (2e) is $O(\Delta x^{2\lceil\frac{s}{2}\rceil-1})$-accurate in general, but is $O(\Delta x^{2\lceil\frac{s}{2}\rceil})$ at $i+\frac{1}{2}$ because the reconstruction stencil $\text{S}_{i+\frac{1}{2},\lceil\frac{s}{2}\rceil-1,\lceil\frac{s}{2}\rceil-1} := \{i+\frac{3}{2}-\lceil\frac{s}{2}\rceil,\cdots,i-\frac{1}{2}+\lceil\frac{s}{2}\rceil\}$. Replacing (2b, 2c, 2d) in (2e), gives the final expression[5]

$$
\begin{aligned}
&[\check{F}_{(vu'),\text{ZRNP},\text{S}_{i,2\lceil\frac{s}{2}\rceil-2,2\lceil\frac{s}{2}\rceil-1}}]_{i+\frac{1}{2}} = \\
&\frac{1}{\Delta x}\sum_{\ell=-\lceil\frac{s}{2}\rceil+1}^{\lceil\frac{s}{2}\rceil-1}\Bigg(\alpha_{R_1,\lceil\frac{s}{2}\rceil-1,\lceil\frac{s}{2}\rceil-1,\ell}(0)\Big(\sum_{p=-\lceil\frac{s}{2}\rceil+1}^{\lceil\frac{s}{2}\rceil}\alpha_{I,\lceil\frac{s}{2}\rceil-1,\lceil\frac{s}{2}\rceil,p}(\tfrac{1}{2})\ v_{i+\ell+p}\Big)\Big(\sum_{q=-\lceil\frac{s}{2}\rceil+1}^{\lceil\frac{s}{2}\rceil}\alpha'_{I,\lceil\frac{s}{2}\rceil-1,\lceil\frac{s}{2}\rceil,q}(\tfrac{1}{2})\ u_{i+\ell+q}\Big)\Bigg) \qquad \text{(2f)}
\end{aligned}
$$

Using the analytical expressions for $\alpha_{R_1,\lceil\frac{s}{2}\rceil-1,\lceil\frac{s}{2}\rceil-1,m}(\xi)$ [21, (45g), p. 287] and for $\alpha_{I,\lceil\frac{s}{2}\rceil-1,\lceil\frac{s}{2}\rceil,p}(\xi)$ [21, (45h), p. 287] it is straightforward to compute the $2\lceil\frac{s}{2}\rceil-1$ rational constants $\alpha_{R_1,\lceil\frac{s}{2}\rceil-1,\lceil\frac{s}{2}\rceil-1,m}(0)$ ($\ell\in\{-\lceil\frac{s}{2}\rceil+1,\cdots,\lceil\frac{s}{2}\rceil-1\}$), the $2\lceil\frac{s}{2}\rceil$ rational constants $\alpha_{I,\lceil\frac{s}{2}\rceil-1,\lceil\frac{s}{2}\rceil,p}(\frac{1}{2})$ ($p\in\{-\lceil\frac{s}{2}\rceil+1,\cdots,\lceil\frac{s}{2}\rceil\}$), and the $2\lceil\frac{s}{2}\rceil$ rational constants $\alpha'_{I,\lceil\frac{s}{2}\rceil-1,\lceil\frac{s}{2}\rceil,q}(\frac{1}{2})$ ($q\in\{-\lceil\frac{s}{2}\rceil+1,\cdots,\lceil\frac{s}{2}\rceil\}$), appearing in the approximation (2f) of the numerical flux $[\check{F}_{(vu'),\text{ZRNP},\text{S}_{i,2\lceil\frac{s}{2}\rceil-2,2\lceil\frac{s}{2}\rceil-1}}]_{i+\frac{1}{2}}$.

2.3 Shen et al. [17]

The scheme of Shen et al. [17] uses the same as Zingg et al. [14] $\text{S}_{i,2\lceil\frac{s}{2}\rceil-2,2\lceil\frac{s}{2}\rceil-1} := \{i-2\lceil\frac{s}{2}\rceil+2,\cdots,i+2\lceil\frac{s}{2}\rceil-1\}$ stencil to compute the numerical flux $[\check{F}_{(vu'),\text{SZC},\text{S}_{i,2\lceil\frac{s}{2}\rceil-2,2\lceil\frac{s}{2}\rceil-1}}]_{i+\frac{1}{2}}$. The 2 schemes are quite similar, except for the approximation of $u'(x_{i+\ell+\frac{1}{2}})$ ($\ell\in\{-\lceil\frac{s}{2}\rceil+1,\cdots,\lceil\frac{s}{2}\rceil-1\}$), for which the entire stencil $\text{S}_{i,2\lceil\frac{s}{2}\rceil-2,2\lceil\frac{s}{2}\rceil-1} := \{i-2\lceil\frac{s}{2}\rceil+2,\cdots,i+2\lceil\frac{s}{2}\rceil-1\}$ is used by Shen et al. [17], $\forall\ell\in\{-\lceil\frac{s}{2}\rceil+1,\cdots,\lceil\frac{s}{2}\rceil-1\}$. Interface fluxes are defined by

$$
\begin{aligned}
[(vu')'_i]_{\text{SZC},\text{S}_{i,2\lceil\frac{s}{2}\rceil-1,2\lceil\frac{s}{2}\rceil-1}} &= \frac{[\check{F}_{(vu'),\text{SZC},\text{S}_{i,2\lceil\frac{s}{2}\rceil-1,2\lceil\frac{s}{2}\rceil-1}}]_{i+\frac{1}{2}} - [\check{F}_{(vu'),\text{SZC},\text{S}_{i-1,2\lceil\frac{s}{2}\rceil-1,2\lceil\frac{s}{2}\rceil-1}}]_{i-\frac{1}{2}}}{\Delta x} \\
&= [(vu')'](x_i) + O(\Delta x^{2\lceil\frac{s}{2}\rceil}) \qquad \text{(3a)}
\end{aligned}
$$

[5] $[\check{vu'}]_{\text{ZRNP},\text{S}_{i,2\lceil\frac{s}{2}\rceil-2,2\lceil\frac{s}{2}\rceil-1}}(x_{i+\ell+\frac{1}{2}}) = p_{I,\lceil\frac{s}{2}\rceil-1,\lceil\frac{s}{2}\rceil-1}(x_{i+\ell+\frac{1}{2}};x_{i+\frac{1}{2}},\Delta x;[\check{vu'}]_{\text{ZRNP},\text{S}_{i+\ell,2\lceil\frac{s}{2}\rceil-2,2\lceil\frac{s}{2}\rceil-1}}) = [\check{v}]_{\text{ZRNP},\text{S}_{i+\ell,\lceil\frac{s}{2}\rceil-1,\lceil\frac{s}{2}\rceil},i+\ell+\frac{1}{2}}[\check{u'}]_{\text{ZRNP},\text{S}_{i+\ell,\lceil\frac{s}{2}\rceil-1,\lceil\frac{s}{2}\rceil},i+\ell+\frac{1}{2}}$ $\forall\ell\in\{-\lceil\frac{s}{2}\rceil+1,\cdots,\lceil\frac{s}{2}\rceil-1\}$ because $\alpha_{I,\lceil\frac{s}{2}\rceil-1,\lceil\frac{s}{2}\rceil-1,\ell}(m)=\delta_{\ell m}$ [23]

Halfpoint values, at the cell-interfaces $i+\ell+\frac{1}{2}$ ($\ell \in \{-\lceil \frac{s}{2} \rceil + 1, \cdots, \lceil \frac{s}{2} \rceil - 1\}$) are defined, using Lagrange interpolation,

$$[\check{v}]_{\mathrm{SZC},\mathrm{S}_{i+\ell,\lceil \frac{s}{2} \rceil - 1,\lceil \frac{s}{2} \rceil},i+\ell+\frac{1}{2}} := [\check{v}]_{\mathrm{ZRNP},\mathrm{S}_{i+\ell,\lceil \frac{s}{2} \rceil - 1,\lceil \frac{s}{2} \rceil},i+\ell+\frac{1}{2}} = (2\mathrm{b}) \tag{3b}$$

$$\begin{aligned}[\check{u'}]_{\mathrm{SZC},\mathrm{S}_{i+\ell,2\lceil \frac{s}{2} \rceil - 2,2\lceil \frac{s}{2} \rceil - 1},i+\ell+\frac{1}{2}} &:= p'_{I,2\lceil \frac{s}{2} \rceil - 2,2\lceil \frac{s}{2} \rceil - 1}(x_i + (\ell+\tfrac{1}{2})\Delta x; x_i, \Delta x; u) \\ &\overset{(1\mathrm{g})}{=} \frac{1}{\Delta x} \sum_{q=-2\lceil \frac{s}{2} \rceil + 2}^{2\lceil \frac{s}{2} \rceil - 1} \alpha'_{I,2\lceil \frac{s}{2} \rceil - 2,2\lceil \frac{s}{2} \rceil - 1,q}(\ell+\tfrac{1}{2})\, u_{i+q} \overset{(1\mathrm{h})}{=} u'(x_{i+\ell+\frac{1}{2}}) + O(\Delta x^{4\lceil \frac{s}{2} \rceil - 3})\end{aligned} \tag{3c}$$

and used to construct the interpolating polynomial of $v(x)u'(x)$, defined by

$$\begin{aligned}[\check{vu'}]_{\mathrm{SZC},\mathrm{S}_{i,2\lceil \frac{s}{2} \rceil - 2,2\lceil \frac{s}{2} \rceil - 1}}(x) &\overset{(1\mathrm{e})}{:=} \sum_{\ell=-\lceil \frac{s}{2} \rceil + 1}^{\lceil \frac{s}{2} \rceil - 1} \Bigg(\alpha_{I,\lceil \frac{s}{2} \rceil - 1,\lceil \frac{s}{2} \rceil - 1,\ell}\Big(\frac{x - x_{i+\frac{1}{2}}}{\Delta x}\Big) \\ &\qquad \Big([\check{v}]_{\mathrm{SZC},\mathrm{S}_{i+\ell,\lceil \frac{s}{2} \rceil - 1,\lceil \frac{s}{2} \rceil},i+\ell+\frac{1}{2}} [\check{u'}]_{\mathrm{SZC},\mathrm{S}_{i+\ell,\lceil \frac{s}{2} \rceil - 1,\lceil \frac{s}{2} \rceil},i+\ell+\frac{1}{2}} \Big) \Bigg) \\ &\overset{(1\mathrm{f},\ 3\mathrm{b},\ 3\mathrm{c})}{=} v(x)u'(x) + O(\Delta x^{2\lceil \frac{s}{2} \rceil})\end{aligned} \tag{3d}$$

Then, this polynomial is reconstructed [21] to obtain the interface fluxes

$$\begin{aligned}[\check{F}_{(vu'),\mathrm{SZC},\mathrm{S}_{i,2\lceil \frac{s}{2} \rceil - 2,2\lceil \frac{s}{2} \rceil - 1}}]_{i+\frac{1}{2}} &:= p_{R_1,\lceil \frac{s}{2} \rceil - 1,\lceil \frac{s}{2} \rceil - 1}(x_{i+\frac{1}{2}}; x_{i+\frac{1}{2}}, \Delta x; [\check{vu'}]_{\mathrm{SZC},\mathrm{S}_{i+\ell,2\lceil \frac{s}{2} \rceil - 2,2\lceil \frac{s}{2} \rceil - 1}}) \\ &= \sum_{\ell=-\lceil \frac{s}{2} \rceil + 1}^{\lceil \frac{s}{2} \rceil - 1} \Big(\alpha_{R_1,\lceil \frac{s}{2} \rceil - 1,\lceil \frac{s}{2} \rceil - 1,\ell}(0) \Big([\check{v}]_{\mathrm{SZC},\mathrm{S}_{i+\ell,\lceil \frac{s}{2} \rceil - 1,\lceil \frac{s}{2} \rceil},i+\ell+\frac{1}{2}} [\check{u'}]_{\mathrm{SZC},\mathrm{S}_{i+\ell,\lceil \frac{s}{2} \rceil - 1,\lceil \frac{s}{2} \rceil},i+\ell+\frac{1}{2}} \Big) \Big) \\ &= [R_{(1;\Delta x)}(vu')](x) + O(\Delta x^{2\lceil \frac{s}{2} \rceil})\end{aligned} \tag{3e}$$

Replacing (3b, 3c, 3d) in (3e), gives in analogy with the scheme of Zingg et al. [14],[5] the final expression

$$\begin{aligned}[\check{F}_{(vu'),\mathrm{SZC},\mathrm{S}_{i,2\lceil \frac{s}{2} \rceil - 2,2\lceil \frac{s}{2} \rceil - 1}}]_{i+\frac{1}{2}} = \frac{1}{\Delta x} \sum_{\ell=-\lceil \frac{s}{2} \rceil + 1}^{\lceil \frac{s}{2} \rceil - 1} \Bigg(&\alpha_{R_1,\lceil \frac{s}{2} \rceil - 1,\lceil \frac{s}{2} \rceil - 1,\ell}(0) \\ &\Big(\sum_{p=-\lceil \frac{s}{2} \rceil + 1}^{s} \alpha_{I,\lceil \frac{s}{2} \rceil - 1,\lceil \frac{s}{2} \rceil,p}(\tfrac{1}{2})\, v_{i+\ell+p} \Big) \Big(\sum_{q=-2\lceil \frac{s}{2} \rceil + 2}^{2\lceil \frac{s}{2} \rceil - 1} \alpha'_{I,2\lceil \frac{s}{2} \rceil - 2,2\lceil \frac{s}{2} \rceil - 1,q}(\ell+\tfrac{1}{2})\, u_{i+q} \Big) \Bigg)\end{aligned} \tag{3f}$$

The difference compared to Zingg et al. [14] is that Shen et al. [17] use a higher-order interpolant for approximating $u'(x)$, but as they correctly state in their paper this reduces the magnitude of the truncation error on a given grid, without improving the order-of-accuracy.

The rational constants $\alpha_{R_1,\lceil \frac{s}{2} \rceil - 1,\lceil \frac{s}{2} \rceil - 1,m}(0)$ ($\ell \in \{-\lceil \frac{s}{2} \rceil + 1, \cdots, \lceil \frac{s}{2} \rceil - 1\}$) and $\alpha_{I,\lceil \frac{s}{2} \rceil - 1,\lceil \frac{s}{2} \rceil,p}(\frac{1}{2})$ ($p \in \{-\lceil \frac{s}{2} \rceil + 1, \cdots, \lceil \frac{s}{2} \rceil\}$) in the expression (3f) of the numerical flux $[\check{F}_{(vu'),\mathrm{SZC},\mathrm{S}_{i,2\lceil \frac{s}{2} \rceil - 2,2\lceil \frac{s}{2} \rceil - 1}}]_{i+\frac{1}{2}}$ are the same as those used in (2f) by Zingg et al. [14]. The new $(2\lceil \frac{s}{2} \rceil - 2) \times (2\lceil \frac{s}{2} \rceil - 1)$ rational constants $\alpha'_{I,2\lceil \frac{s}{2} \rceil - 2,2\lceil \frac{s}{2} \rceil - 1,q}(\ell + \frac{1}{2})$ ($\ell \in \{-\lceil \frac{s}{2} \rceil + 1, \cdots, \lceil \frac{s}{2} \rceil - 1\}$; $q \in \{-2\lceil \frac{s}{2} \rceil + 2, \cdots, 2\lceil \frac{s}{2} \rceil - 1\}$) can be easily calculated using the analytical expression for $\alpha_{I,\lceil \frac{s}{2} \rceil - 1,\lceil \frac{s}{2} \rceil,p}(\xi)$ [21, (45h), p. 287].

2.4 Present scheme

The schemes of Zingg et al. [14] and of Shen et al. [17] yield $O(\Delta x^{2\lceil \frac{s}{2} \rceil})$-accurate approximations of $(vu')'_i$ on the stencil $\mathrm{S}_{i,s,s} := \{i-s, \cdots, i+s\}$, where centred approximations of u''_i by standard finite-differencing yield $O(\Delta x^{2s})$-accuracy [26, (7.6), p. 297]. Examining the method of Zingg et al. [14] (§2.2) it is obvious

that accuracy is limited both by the accuracy of the substencils used for approximating vu' at halfpoints, but also by the final reconstruction from information on $2\lceil\frac{s}{2}\rceil - 1$ discrete values compared to the $2s+1$ available discrete values for v and u on the entire stencil. Shen et al. [17] used higher-order approximations for u', but since the final reconstruction again only uses $2\lceil\frac{s}{2}\rceil - 1$ discrete values for (vu') the resulting scheme is only $O(\Delta x^{2\lceil\frac{s}{2}\rceil})$-accurate. The difficulty with both these approaches [14, 17] lies in the choice made of first approximating vu' at halfpoints, and then finite-differencing [14] or reconstructing [17] to obtain the approximation to $(vu')'$ [14] or to the appropriate fluxes [17]. It turns out that we may obtain $O(\Delta x^{2s})$ accuracy (roughly twice more accurate) on the stencil $\mathrm{S}_{i,s,s} := \{i-s, \cdots, i+s\}$ by simply interpolating $v(x)$ and $u(x)$ on the entire stencil $\mathrm{S}_{i,s-1,s} := \{i-s+1, \cdots, i+s\}$ used for the evaluation of the flux, using all available information at the nodes, and then reconstructing the approximating polynomial of $v(x)u'(x)$ to define the interface fluxes.

To avoid loss of information, and hence order-of-accuracy, we base the present approach for evaluating the flux at $i+\frac{1}{2}$ on the $O(\Delta x^{2s})$-accurate interpolating polynomials $p_{I,s-1,s}(x; x_i, \Delta x; v)$ and $p_{I,s-1,s}(x; x_i, \Delta x; u)$, so that the final approximation

$$[(vu')'_i]_{\mathrm{GV},\mathrm{S}_{i,s,s}} = \frac{[\check{F}_{(vu'),\mathrm{GV},\mathrm{S}_{i,s-1,s}}]_{i+\frac{1}{2}} - [\check{F}_{(vu'),\mathrm{GV},\mathrm{S}_{i-1,s-1,s}}]_{i-\frac{1}{2}}}{\Delta x} = [(vu')'](x_i) + O(\Delta x^{2s}) \tag{4a}$$

uses all information contained in the stencil.

2.4.1 Flux at $i+\frac{1}{2}$ on the general stencil $\mathrm{S}_{i,s-1,s} := \{i-M_-, \cdots, i+M_+\}$

It will prove useful, when working on biased discretizations for near-boundary points, to develop the expression of the flux on the general stencil $\mathrm{S}_{i,s-1,s} := \{i-M_-, \cdots, i+M_+\}$ (1b). We define

$$[\check{v}]_{\mathrm{GV},\mathrm{S}_{i,M_-,M_+}}(x) := \quad p_{I,M_-,M_+}(x; x_i, \Delta x; v) \overset{(1e)}{=} \sum_{p=-M_-}^{M_+} \alpha_{I,M_-,M_+,p}\Big(\frac{x-x_i}{\Delta x}\Big)\, v_{i+p} \overset{(1f)}{=} v(x) + O(\Delta x^{M+1}) \tag{5a}$$

$$[\check{u'}]_{\mathrm{GV},\mathrm{S}_{i,M_-,M_+}}(x) := \frac{d}{dx} p_{I,M_-,M_+}(x; x_i, \Delta x; u) \overset{(1g)}{=} \frac{1}{\Delta x} \sum_{q=-M_-}^{M_+} \alpha'_{I,M_-,M_+,q}\Big(\frac{x-x_i}{\Delta x}\Big)\, u_{i+q} \overset{(1h)}{=} u'(x) + O(\Delta x^{M}) \tag{5b}$$

using Lagrange interpolation on the entire stencil $\mathrm{S}_{i,M_-,M_+} := \{i-M_-, \cdots, i+M_+\}$, and approximate $v(x)u'(x)$ by the product of (5a, 5b)

$$\begin{aligned}[\check{vu'}]_{\mathrm{GV},\mathrm{S}_{i,M_-,M_+}}(x) &:= \frac{1}{\Delta x}\Bigg(\sum_{p=-M_-}^{s} \alpha_{I,M_-,M_+,p}\Big(\frac{x-x_i}{\Delta x}\Big)\, v_{i+p}\Bigg)\Bigg(\sum_{q=-M_-}^{s} \alpha'_{I,M_-,M_+,q}\Big(\frac{x-x_i}{\Delta x}\Big)\, u_{i+q}\Bigg) \\ &\overset{(5a,\,5b)}{=} v(x)u'(x) + O(\Delta x^{M})\end{aligned} \tag{5c}$$

The polynomial (5c) is then reconstructed on S_{i,M_-,M_+}, to define the numerical flux

$$\begin{aligned}[\check{F}_{(vu'),\mathrm{GV},\mathrm{S}_{i,M_-,M_+}}]_{i+\frac{1}{2}} &:= p_{R_1,M_-,M_+}(x; x_{i+\frac{1}{2}}, \Delta x; [\check{vu'}]_{\mathrm{GV},\mathrm{S}_{i,M_-,M_+}}) \\ &\overset{(1g)}{=} \sum_{\ell=-M_-}^{M_+} \alpha_{R_1,M_-,M_+,m}\Big(\frac{x-x_i}{\Delta x}\Big)\, [\check{vu'}]_{\mathrm{GV},\mathrm{S}_{i,M_-,M_+}}(x_i + m\Delta x) \\ &\overset{(1h)}{=} [R_{(1;\Delta x)}(vu')](x) + O(\Delta x^{2s-1})\end{aligned} \tag{5d}$$

so that we have finally

$$[\check{F}_{(vu'),\mathrm{GV},\mathrm{S}_{i,M_-,M_+}}]_{i+\frac{1}{2}} \overset{(5c,\,5d)}{=} \frac{1}{\Delta x}\sum_{p=-M_-}^{M_+}\left(v_{i+p}\sum_{q=-M_-}^{M_+}\underbrace{\left(\alpha_{R_1,M_-,M_+,p}(\tfrac{1}{2})\;\alpha'_{I,M_-,M_+,q}(p)\right)}_{=:\,a_{(vu',\mathrm{GV},M_-,M_+)_{pq}}}u_{i+q}\right) \tag{5e}$$

where we used the well known fact that the fundamental functions of Lagrange interpolation $\alpha_{I,M_-,M_+,p}(\xi)$ are $=0$ at all integer nodes on the stencil ($\forall p\in\{i-M_-,\cdots,i+M_+\}\setminus\{p\}$), except at the node $\xi=p$ where $\alpha_{I,M_-,M_+,p}(p)=1$ [23].

2.4.2 Flux at internal points

At points with sufficient distance from the boundaries so that the points in the stencil $\mathrm{S}_{i,s-1,s}:=\{i-s+1,\cdots,i+s\}$ be defined on the computational grid, *ie* for points $i\in\{s,\cdots,N_i-s\}$, the flux

$$[\check{F}_{(vu'),\mathrm{GV},\mathrm{S}_{i,s-1,s}}]_{i+\frac{1}{2}} \overset{(5e)}{:=} \frac{1}{\Delta x}\sum_{p=-s+1}^{s}\left(v_{i+p}\sum_{q=-s+1}^{s}\left(a_{(vu',\mathrm{GV},s-1,s)_{pq}}\;u_{i+q}\right)\right) \tag{6a}$$

$$a_{(vu',\mathrm{GV},s-1,s)_{pq}} \overset{(5e)}{:=} \alpha_{R_1,s-1,s,p}(\tfrac{1}{2})\;\alpha'_{I,s-1,s,q}(p)\;\in\mathbb{Q}\quad\begin{cases}p\in\{-s+1,\cdots,s\}\\ q\in\{-s+1,\cdots,s\}\end{cases} \tag{6b}$$

is constructed at the interface $i+\frac{1}{2}$. Using the analytical expressions for $\alpha_{R_1,s-1,s-1,m}(\xi)$ [21, (45g), p. 287] and for $\alpha_{I,s-1,s,p}(\xi)$ [21, (45h), p. 287] it is straightforward to compute by (6b) the $(2s)^2$ rational constants $a_{(vu',\mathrm{GV},s-1,s)_{pq}}$ ($p,q\in\{-s+1,\cdots,s\}$) appearing in the definition (6a) of the numerical flux $[\check{F}_{(vu'),\mathrm{GV},\mathrm{S}_{i,s-1,s}}]_{i+\frac{1}{2}}$, which were tabulated for $s\in\{1,\cdots,6\}$ (Tab. 1).

2.5 Remark

It is easy to verify that all of the 3 methods (§2.2, §2.3, and §2.4) yield the same basic $O(\Delta x^2)$ approximation on the stencil $\mathrm{S}_{i,1,1}:=\{i-1,i,i+1\}$ ($s=1\Longrightarrow\lceil\frac{s}{2}\rceil=\lceil\frac{1}{2}\rceil=1=s$)

$$(2\mathrm{f},\,3\mathrm{f},\,6\mathrm{a})\overset{s=1}{\Longrightarrow}[\check{F}_{(vu'),\mathrm{GV},\mathrm{S}_{i,0,1}}]_{i+\frac{1}{2}}=[\check{F}_{(vu'),\mathrm{ZRNP},\mathrm{S}_{i,0,1}}]_{i+\frac{1}{2}}=[\check{F}_{(vu'),\mathrm{SZC},\mathrm{S}_{i,0,1}}]_{i+\frac{1}{2}}=\frac{v_{i+1}+v_i}{2}\frac{u_{i+1}-u_i}{\Delta x} \tag{7}$$

which is widely used in many solvers [8].

2.6 Comparison on $\mathrm{S}_{i,3,3}$

A first computational verification of the 3 schemes was performed (Fig. 2), on the stencil $\mathrm{S}_{i,3,3}:=\{i-3,\cdots,i+3\}$, for 2 sets of functions, $v(x)$ and $u(x)$, studied in Shen et al. [17], SZC1 (§2.8.1) and SZC2 (§2.8.2). Discretization was performed on a uniform grid of N_i points ($N_c=N_i-1$ intervals), using $N_{\mathrm{ph}}=3$ phantom nodes to compute $(vu')'$ at the boundary points, without reverting to biased stencils. The L_∞ norm of the error for these test-cases is defined by the unscaled error

$$E_{L_\infty}(N_c):=\max_{i\in\{1,\cdots,N_c+1\}}|(vu')'_{\mathrm{num}}-(vu')'_{\mathrm{exact}}| \tag{8a}$$

and the associated rate-of-convergence, between 2 consecutive levels of grid refinement, N_c and N_{c_c}, by

$$r_{\mathrm{CNVRG}_{L_\infty}}(N_c):=-\frac{\log_{10}E_{L_\infty}(N_c)-\log_{10}E_{L_\infty}(N_{c_c})}{\log_{10}\left(\frac{N_c}{N_{c_c}}\right)} \tag{8b}$$

All of the 3 schemes achieve their theoretical order-of-accuracy (Fig. 2), $O(\Delta x^4)$ for Zingg et al. [14] and Shen et al. [17], and $O(\Delta x^6)$ for the present method, already at the coarsest grid of $N_i=21$ points

Table 1: Rational constants $a_{(vu',\mathrm{GV},s-1,s)_{pq}} := \alpha_{R_1,s-1,s,p}(\frac{1}{2})\ \alpha'_{I,s-1,s,q}(p) \in \mathbb{Q}$ (6b) appearing in the expression of the numerical flux $[\check{F}_{(vu'),\mathrm{GV},\mathrm{S}_{i,s-1,s}}]_{i+\frac{1}{2}} = \Delta x^{-1} \sum_{p=-s+1}^{s} v_{i+p} \sum_{q=-s+1}^{s} a_{(vu',\mathrm{GV},s-1,s)_{pq}}\ u_{i+q}$ (6a) of the present scheme for the computation of $(vu')'_i$ (4a) ($s \in \{1, \cdots, 6\}$).

	$q=$	-5	-4	-3	-2	-1	0	$+1$	$+2$	$+3$	$+4$	$+5$	$+6$
s	p												
6	-5	$\frac{83711}{153679680}$	$\frac{-1}{504}$	$\frac{5}{1008}$	$\frac{-5}{504}$	$\frac{5}{336}$	$\frac{-1}{60}$	$\frac{1}{72}$	$\frac{-5}{588}$	$\frac{5}{1344}$	$\frac{-5}{4536}$	$\frac{1}{5040}$	$\frac{-1}{60984}$
	-4	$\frac{-67}{304920}$	$\frac{-325687}{69854400}$	$\frac{67}{5544}$	$\frac{-67}{3696}$	$\frac{67}{2772}$	$\frac{-67}{2640}$	$\frac{67}{3300}$	$\frac{-67}{5544}$	$\frac{67}{12936}$	$\frac{-67}{44352}$	$\frac{67}{249480}$	$\frac{-67}{3049200}$
	-3	$\frac{-107}{762300}$	$\frac{107}{34650}$	$\frac{358343}{17463600}$	$\frac{-107}{2310}$	$\frac{107}{2310}$	$\frac{-107}{2475}$	$\frac{107}{3300}$	$\frac{-107}{5775}$	$\frac{107}{13860}$	$\frac{-107}{48510}$	$\frac{107}{277200}$	$\frac{-107}{3430350}$
	-2	$\frac{-443}{3430350}$	$\frac{443}{207900}$	$\frac{-443}{20790}$	$\frac{-329149}{5821200}$	$\frac{443}{3465}$	$\frac{-443}{4950}$	$\frac{443}{7425}$	$\frac{-443}{13860}$	$\frac{443}{34650}$	$\frac{-443}{124740}$	$\frac{443}{727650}$	$\frac{-443}{9147600}$
	-1	$\frac{-5653}{36590400}$	$\frac{5653}{2494800}$	$\frac{-5653}{332640}$	$\frac{5653}{55440}$	$\frac{-5653}{604871}$	$\frac{-5653}{19800}$	$\frac{5653}{39600}$	$\frac{-5653}{83160}$	$\frac{5653}{221760}$	$\frac{-5653}{831600}$	$\frac{5653}{4989600}$	$\frac{-5653}{64033200}$
	0	$\frac{-18107}{64033200}$	$\frac{18107}{4656960}$	$\frac{-18107}{698544}$	$\frac{18107}{155232}$	$\frac{-18107}{5821200}$	$\frac{-18107}{38808}$	$\frac{18107}{27720}$	$\frac{-18107}{77616}$	$\frac{18107}{232848}$	$\frac{-18107}{931392}$	$\frac{18107}{5821200}$	$\frac{-18107}{76839840}$
	$+1$	$\frac{18107}{76839840}$	$\frac{-18107}{5821200}$	$\frac{18107}{931392}$	$\frac{-18107}{232848}$	$\frac{18107}{77616}$	$\frac{-18107}{27720}$	$\frac{18107}{166320}$	$\frac{18107}{38808}$	$\frac{-18107}{155232}$	$\frac{18107}{698544}$	$\frac{-18107}{4656960}$	$\frac{18107}{64033200}$
	$+2$	$\frac{5653}{64033200}$	$\frac{-5653}{4989600}$	$\frac{5653}{831600}$	$\frac{-5653}{221760}$	$\frac{5653}{83160}$	$\frac{-5653}{39600}$	$\frac{5653}{19800}$	$\frac{-604871}{5821200}$	$\frac{-5653}{55440}$	$\frac{5653}{332640}$	$\frac{-5653}{2494800}$	$\frac{5653}{36590400}$
	$+3$	$\frac{443}{9147600}$	$\frac{-443}{727650}$	$\frac{443}{124740}$	$\frac{-443}{34650}$	$\frac{443}{13860}$	$\frac{-443}{7425}$	$\frac{443}{4950}$	$\frac{-443}{3465}$	$\frac{329149}{5821200}$	$\frac{443}{20790}$	$\frac{-443}{207900}$	$\frac{443}{3430350}$
	$+4$	$\frac{107}{3430350}$	$\frac{-107}{277200}$	$\frac{107}{48510}$	$\frac{-107}{13860}$	$\frac{107}{5775}$	$\frac{-107}{3300}$	$\frac{107}{2475}$	$\frac{-107}{2310}$	$\frac{107}{2310}$	$\frac{-358343}{17463600}$	$\frac{-107}{34650}$	$\frac{107}{762300}$
	$+5$	$\frac{67}{3049200}$	$\frac{-67}{249480}$	$\frac{67}{44352}$	$\frac{-67}{12936}$	$\frac{67}{5544}$	$\frac{-67}{3300}$	$\frac{67}{2640}$	$\frac{-67}{2772}$	$\frac{67}{3696}$	$\frac{-67}{5544}$	$\frac{325687}{69854400}$	$\frac{67}{304920}$
	$+6$	$\frac{1}{60984}$	$\frac{-1}{5040}$	$\frac{5}{4536}$	$\frac{-5}{1344}$	$\frac{5}{588}$	$\frac{-1}{72}$	$\frac{1}{60}$	$\frac{-5}{336}$	$\frac{5}{504}$	$\frac{-5}{1008}$	$\frac{1}{504}$	$\frac{-83711}{153679680}$
5	-4		$\frac{-7129}{3175200}$	$\frac{1}{140}$	$\frac{-1}{70}$	$\frac{1}{45}$	$\frac{-1}{40}$	$\frac{1}{50}$	$\frac{-1}{90}$	$\frac{1}{245}$	$\frac{-1}{1120}$	$\frac{1}{11340}$	
	-3		$\frac{23}{22680}$	$\frac{11063}{705600}$	$\frac{-23}{630}$	$\frac{23}{540}$	$\frac{-23}{540}$	$\frac{23}{720}$	$\frac{-23}{1350}$	$\frac{23}{3780}$	$\frac{-23}{17640}$	$\frac{23}{181440}$	
	-2		$\frac{127}{181440}$	$\frac{-127}{10080}$	$\frac{-2159}{39200}$	$\frac{127}{1080}$	$\frac{-127}{1440}$	$\frac{127}{2160}$	$\frac{-127}{4320}$	$\frac{127}{12600}$	$\frac{-127}{60480}$	$\frac{127}{635040}$	
	-1		$\frac{473}{635040}$	$\frac{-473}{47040}$	$\frac{473}{5880}$	$\frac{17501}{151200}$	$\frac{-473}{1680}$	$\frac{473}{3360}$	$\frac{-473}{7560}$	$\frac{473}{23520}$	$\frac{-473}{117600}$	$\frac{473}{1270080}$	
	0		$\frac{1627}{1270080}$	$\frac{-1627}{105840}$	$\frac{1627}{17640}$	$\frac{-1627}{3780}$	$\frac{-1627}{12600}$	$\frac{1627}{2520}$	$\frac{-1627}{7560}$	$\frac{1627}{26460}$	$\frac{-1627}{141120}$	$\frac{1627}{1587600}$	
	$+1$		$\frac{-1627}{1587600}$	$\frac{1627}{141120}$	$\frac{-1627}{26460}$	$\frac{1627}{7560}$	$\frac{-1627}{2520}$	$\frac{1627}{12600}$	$\frac{1627}{3780}$	$\frac{-1627}{17640}$	$\frac{1627}{105840}$	$\frac{-1627}{1270080}$	
	$+2$		$\frac{-473}{1270080}$	$\frac{473}{117600}$	$\frac{-473}{23520}$	$\frac{473}{7560}$	$\frac{-473}{3360}$	$\frac{473}{1680}$	$\frac{-17501}{151200}$	$\frac{-473}{5880}$	$\frac{473}{47040}$	$\frac{-473}{635040}$	
	$+3$		$\frac{-127}{635040}$	$\frac{127}{60480}$	$\frac{-127}{12600}$	$\frac{127}{4320}$	$\frac{-127}{2160}$	$\frac{127}{1440}$	$\frac{-127}{1080}$	$\frac{2159}{39200}$	$\frac{127}{10080}$	$\frac{-127}{181440}$	
	$+4$		$\frac{-23}{181440}$	$\frac{23}{17640}$	$\frac{-23}{3780}$	$\frac{23}{1350}$	$\frac{-23}{720}$	$\frac{23}{540}$	$\frac{-23}{540}$	$\frac{23}{630}$	$\frac{-11063}{705600}$	$\frac{-23}{22680}$	
	$+5$		$\frac{-1}{11340}$	$\frac{1}{1120}$	$\frac{-1}{245}$	$\frac{1}{90}$	$\frac{-1}{50}$	$\frac{1}{40}$	$\frac{-1}{45}$	$\frac{1}{70}$	$\frac{-1}{140}$	$\frac{7129}{3175200}$	
4	-3			$\frac{363}{39200}$	$\frac{-1}{40}$	$\frac{3}{80}$	$\frac{-1}{24}$	$\frac{1}{32}$	$\frac{-3}{200}$	$\frac{1}{240}$	$\frac{-1}{1960}$		
	-2			$\frac{-29}{5880}$	$\frac{-841}{16800}$	$\frac{29}{280}$	$\frac{-29}{336}$	$\frac{29}{504}$	$\frac{-29}{1120}$	$\frac{29}{4200}$	$\frac{-29}{35280}$		
	-1			$\frac{-139}{35280}$	$\frac{139}{2520}$	$\frac{6533}{50400}$	$\frac{-139}{504}$	$\frac{139}{1008}$	$\frac{-139}{2520}$	$\frac{139}{10080}$	$\frac{-139}{88200}$		
	0			$\frac{-533}{88200}$	$\frac{533}{8400}$	$\frac{-533}{1400}$	$\frac{-533}{3360}$	$\frac{533}{840}$	$\frac{-533}{2800}$	$\frac{533}{12600}$	$\frac{-533}{117600}$		
	$+1$			$\frac{533}{117600}$	$\frac{-533}{12600}$	$\frac{533}{2800}$	$\frac{-533}{840}$	$\frac{533}{3360}$	$\frac{-533}{1400}$	$\frac{-533}{8400}$	$\frac{533}{88200}$		
	$+2$			$\frac{139}{88200}$	$\frac{-139}{10080}$	$\frac{139}{2520}$	$\frac{-139}{1008}$	$\frac{139}{504}$	$\frac{-6533}{50400}$	$\frac{-139}{2520}$	$\frac{139}{35280}$		
	$+3$			$\frac{29}{35280}$	$\frac{-29}{4200}$	$\frac{29}{1120}$	$\frac{-29}{504}$	$\frac{29}{336}$	$\frac{-29}{280}$	$\frac{841}{16800}$	$\frac{29}{5880}$		
	$+4$			$\frac{1}{1960}$	$\frac{-1}{240}$	$\frac{3}{200}$	$\frac{-1}{32}$	$\frac{1}{24}$	$\frac{-3}{80}$	$\frac{1}{40}$	$\frac{-363}{39200}$		
3	-2				$\frac{-137}{3600}$	$\frac{1}{12}$	$\frac{-1}{12}$	$\frac{1}{18}$	$\frac{-1}{48}$	$\frac{1}{300}$			
	-1				$\frac{2}{75}$	$\frac{13}{90}$	$\frac{-4}{15}$	$\frac{2}{15}$	$\frac{-2}{45}$	$\frac{1}{150}$			
	0				$\frac{37}{1200}$	$\frac{-37}{120}$	$\frac{-37}{180}$	$\frac{37}{60}$	$\frac{-37}{240}$	$\frac{37}{1800}$			
	$+1$				$\frac{-37}{1800}$	$\frac{37}{240}$	$\frac{-37}{60}$	$\frac{37}{180}$	$\frac{37}{120}$	$\frac{-37}{1200}$			
	$+2$				$\frac{-1}{150}$	$\frac{2}{45}$	$\frac{-2}{15}$	$\frac{4}{15}$	$\frac{-13}{90}$	$\frac{-2}{75}$			
	$+3$				$\frac{-1}{300}$	$\frac{1}{48}$	$\frac{-1}{18}$	$\frac{1}{12}$	$\frac{-1}{12}$	$\frac{137}{3600}$			
2	-1					$\frac{11}{72}$	$\frac{-1}{4}$	$\frac{1}{8}$	$\frac{-1}{36}$				
	0					$\frac{-7}{36}$	$\frac{-7}{24}$	$\frac{7}{12}$	$\frac{-7}{72}$				
	$+1$					$\frac{7}{72}$	$\frac{-7}{12}$	$\frac{7}{24}$	$\frac{7}{36}$				
	$+2$					$\frac{1}{36}$	$\frac{-1}{8}$	$\frac{1}{4}$	$\frac{-11}{72}$				
2	0						$\frac{-1}{2}$	$\frac{+1}{2}$					
	$+1$						$\frac{-1}{2}$	$\frac{+1}{2}$					

(Fig. 2). More interestingly, the present scheme systematically has a lower error, even on the coarsest grid. Improvement by the present method is higher for the SZC2 (§2.8.2) test-case (Fig. 2), for which $u(x)$ is a wavy function.

To obtain an $O(\Delta x^{2s})$ accuracy, the stencil width increases linearly with s, and the computational

complexity increases quadratically with s (Tab. 2). If the 3 methods are compared, for the same order-of-accuracy (Tab. 2), it is seen that, for large s, the present method obtains the same accuracy as the previously published approaches [14, 17], on an asymptotically twice more compact stencil, and with roughly half the computational complexity.

Table 2: Number of numerical constants (cooefficients) appearing in the schemes of Zingg et al. [14] (2f), of Shen et al. [17] (3f), and in the present method (6), computational complexity (number of both additions and multiplications), and discretization stencil-width, at interior points.

scheme	order	number of coefficients	complexity	stencil-width
ZNRP [14]	$O(\Delta x^{2s})$	$6s-1$	$16s^2-1$	$4s-2$
SZC [17]	$O(\Delta x^{2s})$	$4s^2-2s+1$	$24s^2-18s+3$	$4s-2$
present	$O(\Delta x^{2s})$	$4s^2$	$8s^2+2s-1$	$2s$

2.7 Near-boundary points

When $i \leq s-1$ or $i \geq N_{i-s}$ there are not enough points in the computational domain to compute the flux $[\check{F}_{(vu'),\mathrm{GV},\mathrm{S}_{i,s-1,s}}]_{i+\frac{1}{2}}$ (6) and one must use biased stencils. The near-boundary interfaces, in the neighbourhood of the boundary $i=1$, requiring biased stencils, are

$$\{\underbrace{0+\tfrac{1}{2}}_{1-\frac{1}{2}}, 1+\tfrac{1}{2}, \cdots, (s-1)+\tfrac{1}{2}\} = \{s-\ell_\mathrm{b}+\tfrac{1}{2}\ ;\ \ell_\mathrm{b}=s,\cdots,1\} \tag{9a}$$

For these interfaces (9a), we use the stencils

$$0+\tfrac{1}{2}=1-\tfrac{1}{2} \ :\ \{\underbrace{1}_{=0-(-1)}, \cdots, \underbrace{2s+1}_{=0+(2s+1)}\} = \mathrm{S}_{0,-1,2s+1} \tag{9b}$$

$$1+\tfrac{1}{2} \ :\ \{\underbrace{1}_{=1-0}, \cdots, \underbrace{2s+1}_{=1+(2s)}\} = \mathrm{S}_{1,0,2s} \tag{9c}$$

$$2+\tfrac{1}{2} \ :\ \{\underbrace{1}_{=2-1}, \cdots, \underbrace{2s+1}_{=2+(2s-1)}\} = \mathrm{S}_{2,1,2s-1} \tag{9d}$$

$$\vdots$$

$$s-1+\tfrac{1}{2} \ :\ \{\underbrace{1}_{=(s-1)-(s-2)}, \cdots, \underbrace{2s+1}_{=(s-1)+(s+2)}\} = \mathrm{S}_{s-1,s-2,s+2} \tag{9e}$$

ie the same set of points, $\{1,\cdots,2s+1\}$, to compute the flux. The stencil $\{1,\cdots,2s+1\}$ includes one more cell in the stencil with compared to internal points (§2.4.2). Symmetrically, the set $\{N_{i-2s},\cdots,N_i\}$ is used for the interfaces

$$\{N_i+\tfrac{1}{2}, N_i-1+\frac{1}{2}, N_i-2+\tfrac{1}{2}, \cdots, N_i-(s-1)+\tfrac{1}{2}\} = \{N_i-(s-\ell_\mathrm{b})+\tfrac{1}{2}\ ;\ \ell_\mathrm{b}=s,\cdots,1\} \tag{9f}$$

near the boundary $i=N_i$. For both boundaries (9a, 9f), $\ell_\mathrm{b}=s$ corresponds to completely extrapolated interfaces (outside of the computational domain).

2.8 Computational examples

To demonstrate that the proposed scheme achieves its theoretical order-of-accuracy, we first examine the numerical computation of $\Big(v(x)u'(x)\Big)'$ for several test-functions (§2.8.1–§2.8.2). Then, we apply the proposed scheme to the computation of laminar Couette flow of air (§2.8.3).

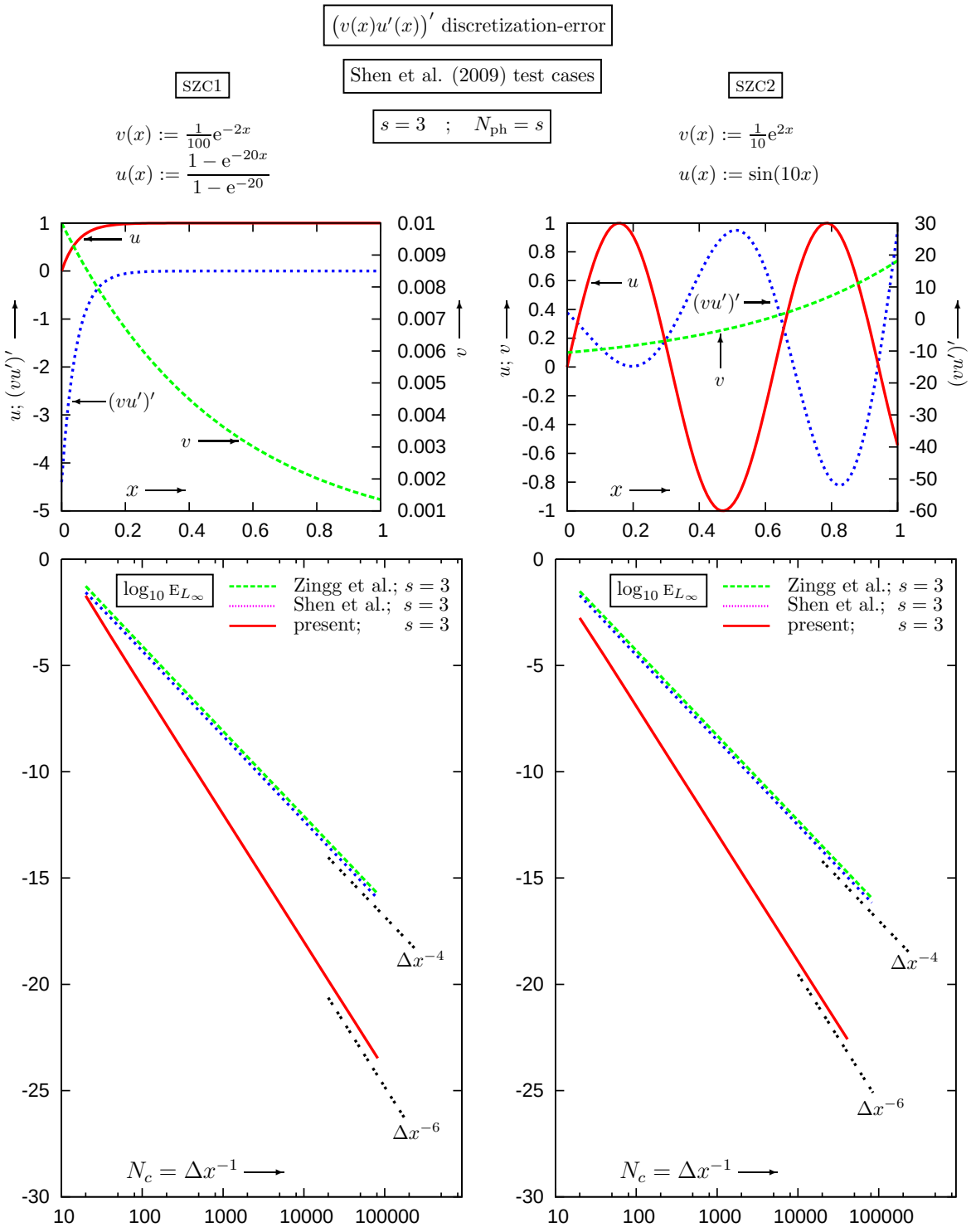

Figure 2: L_∞-norm error E_{L_∞} (8a), as a function of the number of grid-cells $N_c = N_j - 1$, of the numerical approximation of $(vu')'$ on the stencil $\mathrm{s}_{i,3,3} := \{i-3, \cdots, i+3\}$ by the present method (4a, 6), for the test-cases (10, 11) of Shen et al. [17], using progressively refined computational grids ($N_i = 21, 41, 81, 161, 321, 641, 1281, 2561, 5121, 10241, 20481, 40961, 81921$ points) with $N_{\rm ph} = 3$ phantom nodes, and comparison with the previous approaches of Zingg et al. [14] (2a, 2f) and of Shen et al. [17] (3a, 3f).

2.8.1 $v(x) := \frac{1}{100}\mathrm{e}^{-2x}$, $u(x) := (1-\mathrm{e}^{-20})^{-1}(1-\mathrm{e}^{-20x})$; $x \in [0,1]$

This test-case studied by Shen et al. [17]

$$\left.\begin{array}{l} u(x) := \sin 10x \\ v(x) := \frac{1}{10}\mathrm{e}^{2x} \end{array}\right\} \Longrightarrow (v(x)u'(x))' = \frac{-22\mathrm{e}^{-22x}}{5(1-\mathrm{e}^{-20})} \tag{10}$$

The proposed scheme either $N_{\mathrm{ph}} = s$ phantom nodes to the mesh to avaoid the use of biased stencils or $N_{\mathrm{ph}} = 1$ phantom node, achieves the theoretical order-of-accuracy for $s \in \{1, \cdots, 9\}$ (Fig. 3).

2.8.2 $v(x) := \frac{1}{10}\mathrm{e}^{2x}$, $u(x) := \sin 10x$; $x \in [0,1]$

This test-case studied by Shen et al. [17]

$$\left.\begin{array}{l} u(x) := \sin 10x \\ v(x) := \frac{1}{10}\mathrm{e}^{2x} \end{array}\right\} \Longrightarrow (v(x)u'(x))' = -2\mathrm{e}^{2x}(5\sin 10x - \cos 10x) \tag{11}$$

Again the scheme achieves its theoretical order-of-accuracy for $s \in \{1, \cdots, 9\}$ (Fig. 4).

2.8.3 Laminar compressible Couette flow

For laminar compressible fully developed Couette flow [27, pp. 190–192] between a fixed adiabatic wall at $y = 0$ and a moving isothermal wall at $y = \delta$, the compressible Navier-Stokes equations [27, pp. 190–192] simplify (under the assumption of fully developed unidirectional flow parallel to the 2 plates, $\vec{V} = u(y)\vec{e}_x$, which satisfies automatically the steady continuity equation) to

$$p = \text{const} \tag{12a}$$

$$0 = \frac{d}{dy}\left(\mu(T)\frac{du}{\partial y}\right) \tag{12b}$$

$$0 = \mu(T)\left(\frac{du}{dy}\right)^2 + \frac{d}{dy}\left(\lambda(T)\frac{dT}{dy}\right) \tag{12c}$$

where y is the coordinate normal to the plates and to the flow, u is the x-wise velocity-component, T is the temperature, $\mu(T)$ is the dynamic coefficient of viscosity depending on T [28], $\lambda(T)$ is the coefficient of heat conductivity depending on T [28]. We consider flow of air, with

$$\mu(T) \overset{[28]}{=} \mu_0 \left[\frac{T}{T_{\mu_0}}\right]^{\frac{3}{2}} \frac{S_\mu + T_{\mu_0}}{S_\mu + T}\ ; \quad \mu_0 = \mu(T_{\mu_0}) = 17.11 \times 10^{-6}\ \mathrm{Pa}\ s\ ; \quad T_{\mu_0} = 273.15\ \mathrm{K}\ ; \quad S_\mu = 110.4\ \mathrm{K} \tag{12d}$$

$$\lambda(T) \overset{[28]}{=} \lambda_0 \frac{\mu(T)}{\mu_0}[1 + A_\lambda(T - T_{\mu_0})]\ ; \quad \lambda_0 = \lambda(T_{\mu_0}) = 0.0242\ \mathrm{W\ m^{-1}\ K^{-1}}\ ; \quad A_\lambda = 0.00023\ \mathrm{K^{-1}}; \tag{12e}$$

Under the assumption that μ (12d) and λ (12e) are functions of T only, (12) is a system of 2 ODEs (12b, 12c) for the 2 variables u and T, with boundary-conditions

$$u(0) = 0 \tag{13a}$$

$$\frac{dT}{dy}(0) = 0 \tag{13b}$$

$$u(\delta) = u_e > 0 \tag{13c}$$

$$T(\delta) = T_e > 0 \tag{13d}$$

The derivatives $d_y(\mu(T)d_y u)$ in (12b) and $d_y(\lambda(T)d_y T)$ in (12c) are discretized using the present method on the stencil $\mathrm{s}_{i,s,s} := \{i-s, \cdots, i+s\}$ for interior points (§2.4), which provides $O(\Delta x^{2s})$ accuracy, and appropriately biased stencils at near-boundary points (§2.7), reducing the theoretical order-of-accuracy to

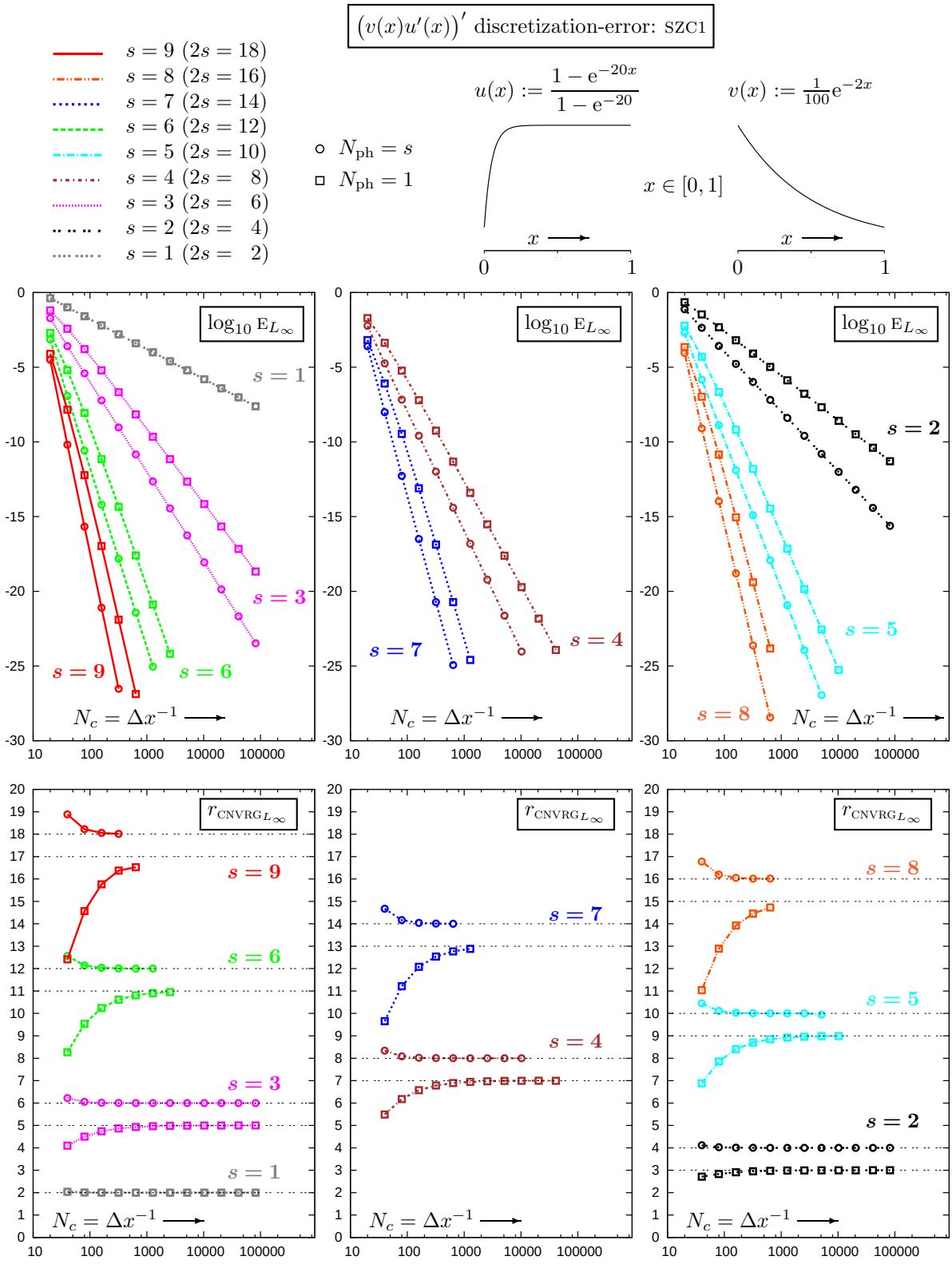

Figure 3: L_∞-norm error E_{L_∞} (8a) and rate-of-convergence $r_{\text{CNVRG}_{L_\infty}}$ (8b), as a function of the number of grid-cells $N_c = N_j - 1$, of the numerical approximation of $(vu')'$ by the present method (6, 9) with $s \in \{1, \cdots, 9\}$, for the SZC1 test-case (10) of Shen et al. [17], using $N_{\text{ph}} \in \{1, s\}$ phantom nodes on progressively refined computational grids ($N_i = 21, 41, 81, 161, 321, 641, 1281, 2561, 5121, 10241, 20481, 40961, 81921$ points depending on the value of the order-parameter s).

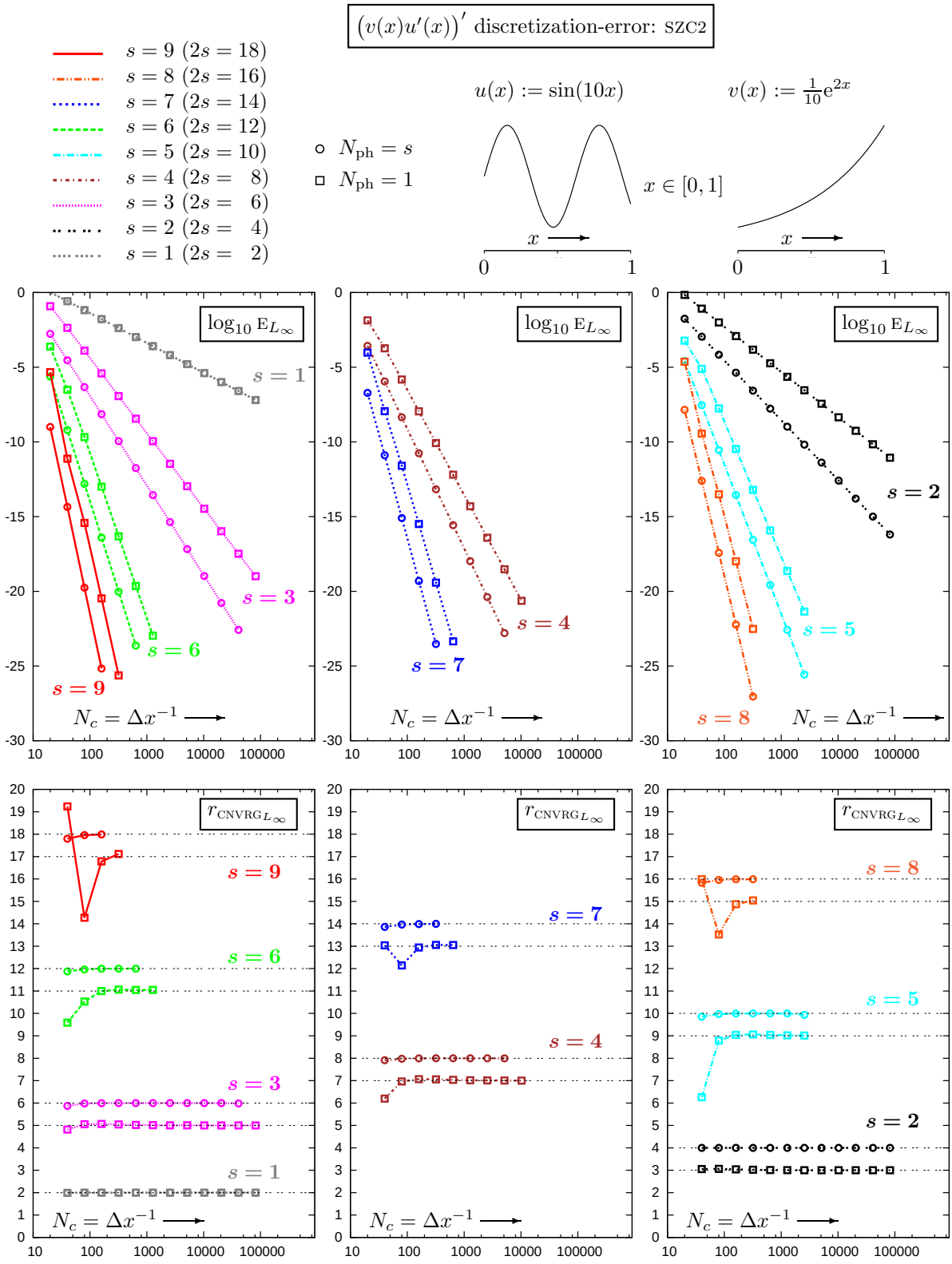

Figure 4: L_∞-norm error E_{L_∞} (8a) and rate-of-convergence $r_{\text{CNVRG}_{L_\infty}}$ (8b), as a function of the number of grid-cells $N_c = N_j - 1$, of the numerical approximation of $(vu')'$ by the present method (6, 9) with $s \in \{1, \cdots, 9\}$, for the SZC2 test-case (11) of Shen et al. [17], using $N_{\text{ph}} \in \{1, s\}$ phantom nodes on progressively refined computational grids ($N_i = 21, 41, 81, 161, 321, 641, 1281, 2561, 5121, 10241, 20481, 40961, 81921$ points depending on the value of s).

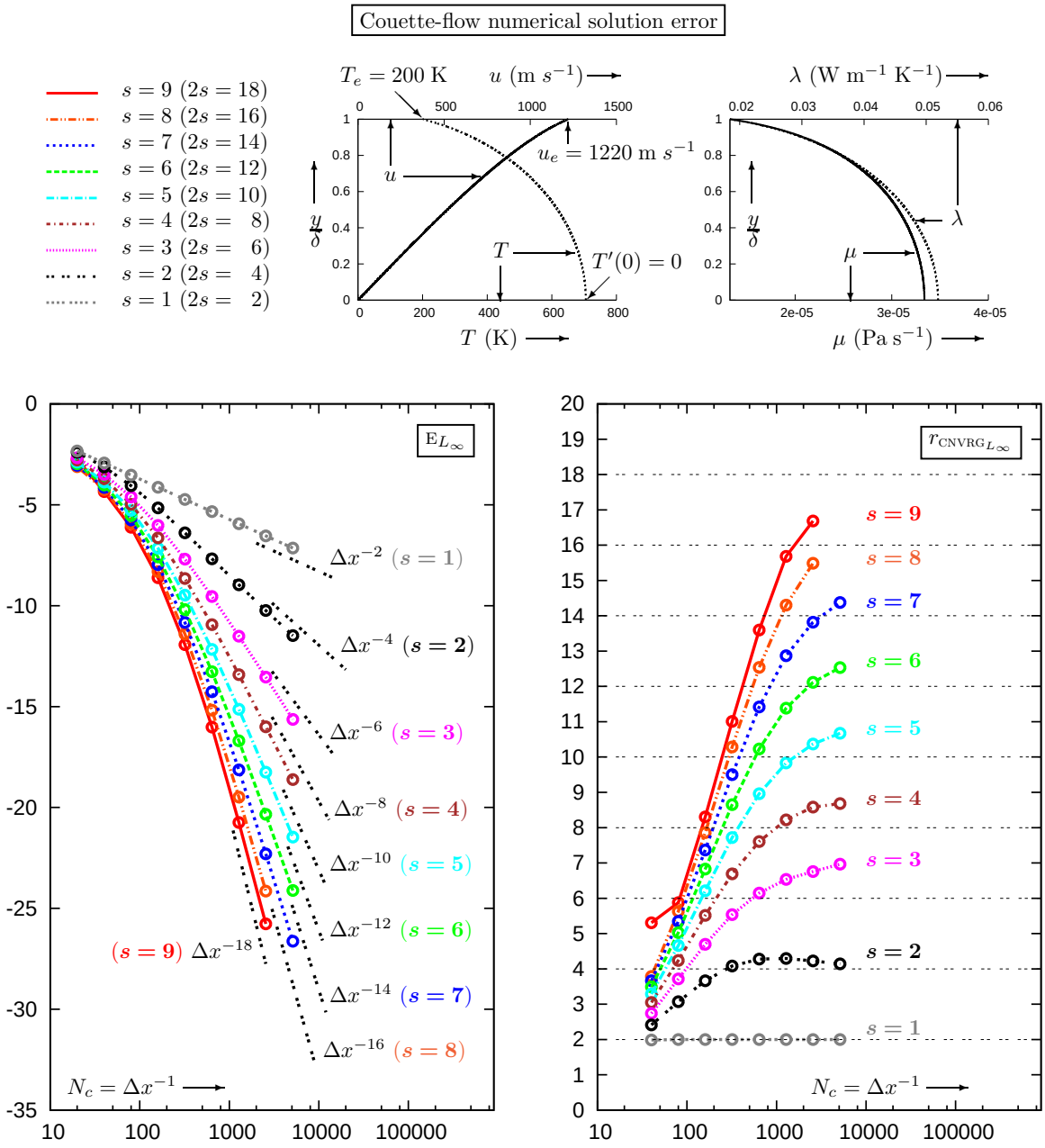

Figure 5: L_∞-norm error E_{L_∞} (15) and rate-of-convergence $r_{\mathrm{CNVRG}_{L_\infty}}$ (8b), as a function of the number of grid-cells $N_c = N_j - 1$, for the difference from the analytical solution of numerical computations of compressible laminar Couette flow, using the present method (14) for $s = 1, \cdots, 9$, on progressively refined computational grids ($N_x = 21, 41, 81, 161, 321, 641, 1281, 2561, 5121$ points).

$O(\Delta x^{2s-1})$. The derivative $d_y u$ appearing in the source-term $\mu(T)(d_y u)^2$, representing heating due to viscous friction in (12c), is discretized using standard centered $O(\Delta y^{2s})$ finite-differences [29] on the stencil $\mathrm{S}_{i,s,s} := \{i-s, \cdots, i+s\}$ for interior points, and using $O(\Delta y^{2s})$ biased finite-differences at the near-boundary-points. The adiabatic-wall boundary-condition (13a) is also discretized using biased $O(\Delta y^{2s})$ finite-differences. The global accuracy is therefore $O(\Delta y^{2s-1})$ for $s \geq 2$, and $O(\Delta y^2)$ for $s = 1$ for which all points, except at the

walls where BCs are applied instead, are internal points.

A homogeneous grid of N_j points ($j = 1$ is the lower fixed adiabatic wall, $j = N_j$ is the upper isothermal wall, $(N_j - 1)\Delta y = \delta$). The flow is initialized by

$$u_{0,j} = \frac{y_j}{\delta} u_e \tag{14a}$$

$$T_{0,j} = T_e \tag{14b}$$

and the nonlinear algebraic system of equations

$$\frac{[\check{F}_{(\mu d_y u),\mathrm{GV},\mathrm{S}_{i,s-1,s}}]_{i+\frac{1}{2}} - [\check{F}_{(\mu d_y u),\mathrm{GV},\mathrm{S}_{i,s-1,s}}]_{i-\frac{1}{2}}}{\Delta y} = 0 \tag{14c}$$

$$\mu(T_{n,j}) \left[\frac{du}{dy}\right]_j^2 + \frac{[\check{F}_{(\lambda d_y T),\mathrm{GV},\mathrm{S}_{i,s-1,s}}]_{i+\frac{1}{2}} - [\check{F}_{(\lambda d_y T),\mathrm{GV},\mathrm{S}_{i,s-1,s}}]_{i-\frac{1}{2}}}{\Delta y} = 0 \tag{14d}$$

are solved using quasi-Newton iteration based on an $O(\Delta x^2)$ approximate Jacobian, corresponding to an $O(\Delta x^2)$ discretization on the restricted stencil $\mathrm{S}_{i,1,1}$ [30].

Numerical results were obtained for $s \in \{1, \cdots, 9\}$, on progressively finer grids (Fig. 5), and their accuracy was assessed by comparison with the semi-analytical solution of (12, 13), which was determined with a precision better than 30 significant digits. Since the problem (12, 13) involves 2 variables (u and T), we used the nondimensional error-norm

$$E_{L_\infty}(N_c) := \max_{j \in \{1,\cdots,N_c+1\}} \left(\frac{|u_{\mathrm{num}} - u_{\mathrm{exact}}|}{u_e}, \frac{|T_{\mathrm{num}} - T_{\mathrm{exact}}|}{T_e} \right) \tag{15}$$

function of the number of grid-cells $N_c = N_j - 1$. This norm (15) was then used in (8b) to compute the rate-of-convergence (Fig. 5).

For all of the studied values of the order-parameter $s \in \{1, \cdots, 9\}$, the scheme reaches its theoretical order-of-accuracy (Fig. 5), the $s = 9$ scheme reaching numerical noise after $N_c = 2560$ cells, where $r_{\mathrm{CNVRG}_{L_\infty}}(N_c = 2560, s = 9) \approxeq 17$. It appears indeed that, for this particular problem, and for the range of grids used, the method is superconvergent, reaching and exceeding $O(\Delta x^{2s})$ order-of-accuracy (Fig. 5), whereas $O(\Delta x^{2s-1})$ order-of-accuracy is expected, because of the biased stencils used at the near-boundary-points.

3 Multidimensional extension

3.1 Viscous stresses in the Navier-Stokes equations

For a standard Newtonian constitutive relation, the viscous stress tensor $\boldsymbol{\tau}$ is of the form

$$\boldsymbol{\tau} = 2\mu \mathbf{S} + \left(\mu_{\mathrm{B}} - \tfrac{2}{3}\mu\right) \mathrm{tr}(\mathbf{S}) \mathbf{I}_3 \tag{16a}$$

where $\mathbf{S} := \frac{1}{2}\left(\mathrm{grad}\vec{V} + (\mathrm{grad}\vec{V})^{\mathrm{T}}\right)$ is the rate-of-strain tensor, $\mu = \mu(\rho, T)$ is the dynamic viscosity, $\mu_{\mathrm{B}} = \mu_{\mathrm{B}}(\rho, T)$ is the bulk viscosity, $\mathbf{I}_3$ is the identity tensor in the Euclidian 3-D space $\mathbb{E}^3$, ρ is the fluid density and T the static temperature. As a consequence, the viscous force per unit volume $\mathrm{div}\boldsymbol{\tau}$ reads, by straightforward computation,

$$\begin{aligned} \mathrm{div}\boldsymbol{\tau} = \Bigg[& \frac{\partial}{\partial x}\left(\left(\mu_{\mathrm{B}} + \tfrac{4}{3}\mu\right)\frac{\partial u}{\partial x}\right) + \frac{\partial}{\partial y}\left(\mu\frac{\partial u}{\partial y}\right) + \frac{\partial}{\partial z}\left(\mu\frac{\partial u}{\partial z}\right) \\ & \underbrace{+ \frac{\partial}{\partial x}\left(\left(\mu_{\mathrm{B}} - \tfrac{2}{3}\mu\right)\left(\frac{\partial v}{\partial y} + \frac{\partial w}{\partial z}\right)\right) + \frac{\partial}{\partial y}\left(\mu\frac{\partial v}{\partial x}\right) + \frac{\partial}{\partial z}\left(\mu\frac{\partial w}{\partial x}\right)}_{\text{cross-derivatives}} \Bigg] \vec{e}_x \end{aligned}$$

$$
\begin{aligned}
&+\left[\frac{\partial}{\partial x}\left(\mu\frac{\partial v}{\partial x}\right)+\frac{\partial}{\partial y}\left(\left(\mu_{\text{B}}+\tfrac{4}{3}\mu\right)\frac{\partial v}{\partial y}\right)+\frac{\partial}{\partial z}\left(\mu\frac{\partial v}{\partial z}\right)\right.\\
&\left.+\underbrace{\frac{\partial}{\partial x}\left(\mu\frac{\partial u}{\partial y}\right)+\frac{\partial}{\partial y}\left(\left(\mu_{\text{B}}-\tfrac{2}{3}\mu\right)\left(\frac{\partial w}{\partial z}+\frac{\partial u}{\partial x}\right)\right)+\frac{\partial}{\partial z}\left(\mu\frac{\partial w}{\partial y}\right)}_{\text{cross-derivatives}}\right]\vec{e}_y\\
&+\left[\frac{\partial}{\partial x}\left(\mu\frac{\partial w}{\partial x}\right)+\frac{\partial}{\partial y}\left(\mu\frac{\partial w}{\partial y}\right)+\frac{\partial}{\partial z}\left(\left(\mu_{\text{B}}+\tfrac{4}{3}\mu\right)\frac{\partial w}{\partial z}\right)\right.\\
&\left.+\underbrace{\frac{\partial}{\partial x}\left(\mu\frac{\partial u}{\partial z}\right)+\frac{\partial}{\partial y}\left(\mu\frac{\partial v}{\partial z}\right)+\frac{\partial}{\partial z}\left(\left(\mu_{\text{B}}-\tfrac{2}{3}\mu\right)\left(\frac{\partial u}{\partial x}+\frac{\partial v}{\partial y}\right)\right)}_{\text{cross-derivatives}}\right]\vec{e}_z
\end{aligned}
\tag{16b}
$$

and contains both terms which can be discretized using the previously developed scheme for $(v(x)u(x))'$ and cross-derivatives, *eg* $\partial_x(\mu\partial_y u)$, which require a different method. It turns out that the discretization of cross-derivatives is simpler than the method (§ 2.4) required to discretize the linewise derivatives x, *eg* $\partial_x(\mu\partial_x u)$.

For a fluid with a Newtonian constitutive relation (16a) and following a linear Fourier heat-flux law

$$
\vec{q}=-\lambda(\rho,T)\text{grad}T \tag{16c}
$$

where $\vec{q}$ is the heat-flux vector, the power per unit volume due to friction and heat conduction reads, by straightforward differentiation

$$
\begin{aligned}
\text{div}\left(\vec{V}.\boldsymbol{\tau}-\vec{q}\right)=&\frac{\partial}{\partial x}\left[\left(\mu_{\text{B}}+\tfrac{4}{3}\mu\right)u\frac{\partial u}{\partial x}+\mu v\frac{\partial v}{\partial x}+\mu w\frac{\partial w}{\partial x}-\lambda\frac{\partial T}{\partial x}\right]\\
&+\underbrace{\frac{\partial}{\partial x}\left[\left(\mu_{\text{B}}-\tfrac{2}{3}\mu\right)u\left(\frac{\partial v}{\partial y}+\frac{\partial w}{\partial z}\right)+\mu v\frac{\partial u}{\partial y}+\mu w\frac{\partial u}{\partial z}\right]}_{\text{cross-derivatives}}\\
&+\frac{\partial}{\partial y}\left[\mu u\frac{\partial u}{\partial y}+\left(\mu_{\text{B}}+\tfrac{4}{3}\mu\right)v\frac{\partial v}{\partial y}+\mu w\frac{\partial w}{\partial y}-\lambda\frac{\partial T}{\partial y}\right]\\
&+\underbrace{\frac{\partial}{\partial y}\left[\mu u\frac{\partial v}{\partial x}+\left(\mu_{\text{B}}-\tfrac{2}{3}\mu\right)v\left(\frac{\partial u}{\partial x}+\frac{\partial w}{\partial z}\right)+\mu w\frac{\partial v}{\partial z}\right]}_{\text{cross-derivatives}}\\
&+\frac{\partial}{\partial z}\left[\mu u\frac{\partial u}{\partial z}+\mu v\frac{\partial v}{\partial z}+\left(\mu_{\text{B}}+\tfrac{4}{3}\mu\right)w\frac{\partial w}{\partial z}-\lambda\frac{\partial T}{\partial z}\right]\\
&+\underbrace{\frac{\partial}{\partial z}\left[\mu u\frac{\partial w}{\partial x}+\mu v\frac{\partial w}{\partial y}+\left(\mu_{\text{B}}-\tfrac{2}{3}\mu\right)w\left(\frac{\partial u}{\partial x}+\frac{\partial v}{\partial y}\right)\right]}_{\text{cross-derivatives}}
\end{aligned}
\tag{16d}
$$

3.2 Numerical fluxes for cross-derivatives ($\partial_x(v\partial_y u)$)

The approach followed for the discretization of cross-derivatives is a generalization to higher-order of accurarcy of the method used by Zingg et al. [14] and Shen et al. [17]. First, the derivative $\partial_y u$ is approximated at the points of the computational grid[6] using standard centered $O(\Delta x^{2s})$ finite-differencing (equivalently differentiation of the Lagrange interpolating polynomial on the stencil

$$
\left[\left[\check{\partial_y u}\right]_{\text{S}\binom{i,0,0}{j,s,s}{k,0,0}}\right]_{ijk}\overset{(1\text{g})}{:=}\frac{1}{\Delta y}\sum_{\ell=-s}^{+s}\alpha'_{I,s,s,\ell}(0)u_{i,j+\ell,k}\overset{(1\text{h})}{=}\left.\frac{\partial u}{\partial y}\right|_{ijk}+O(\Delta y^{2s}) \tag{17a}
$$

[6] the direction i,j,k of the homogeneous Cartesian grid used, are aligned with the x,y,z directions of the Cartesian system of coordinates.

on the stencil

$$\mathrm{S}\begin{pmatrix} i,0,0 \\ j,s,s \\ k,0,0 \end{pmatrix} := \big\{ (i, j-s, k), \cdots, (i, j+s, k) \big\} \tag{17b}$$

where, as usual, the $O(\Delta y^{2s-1})$ accuracy of the derivative of the Lagrange interpolating polynomial becomes $O(\Delta y^{2s})$ at the point ijk, because the stencil is centered with respect to this point [26, (7.6), p. 297]. Then, the Lagrange interpolating polynomial

$$\begin{aligned} \big[v\check{\partial}_y u\big]_{\mathrm{S}\begin{pmatrix} i,s-1,s \\ j,s\ \ ,s \\ k,0\ \ ,0 \end{pmatrix},j,k} (x_i + \xi\Delta x) &\overset{(1e)}{:=} \sum_{\ell=-s+1}^{+s} \alpha_{I,s-1,s,\ell}(\xi)\ v_{i+\ell,j,k} \left[[\check{\partial_y} u]_{\mathrm{S}\begin{pmatrix} i+\ell,0,0 \\ j\ \ ,s,s \\ k\ \ ,0,0 \end{pmatrix}} \right]_{i+\ell,j,k} \\ &\overset{(1f,\ 16a)}{=} [v\partial_y u]_{jk} (x_i + \xi\Delta x) + O(\Delta x^{2s-1}, \Delta y^{2s}) \end{aligned} \tag{17c}$$

is reconstructed to obtain the required flux

$$\begin{aligned} \left[\check{F}_{(v\partial_y u),\mathrm{S}\begin{pmatrix} i,s-1,s \\ j,s\ \ ,s \\ k,0\ \ ,0 \end{pmatrix}} \right]_{i+\frac{1}{2},j,k} &:= p_{R_1,s-1,s} \left(x_i + \tfrac{1}{2}\Delta x; x_i, \Delta x; \big[v\check{\partial}_y u\big]_{\mathrm{S}\begin{pmatrix} i,s-1,s \\ j,s\ \ ,s \\ k,0\ \ ,0 \end{pmatrix},j,k} \right) \\ &\overset{(1i,\ ??)}{=} \sum_{\ell=-s+1}^{+s} \alpha_{R_1,s-1,s,\ell}(\tfrac{1}{2})\ v_{i+\ell,j,k} \left[[\check{\partial}_y u]_{\mathrm{S}\begin{pmatrix} i+\ell,0,0 \\ j\ \ ,s,s \\ k\ \ ,0,0 \end{pmatrix}} \right]_{i+\ell,j,k} \\ &\overset{(1f,\ 16a)}{=} \big[R_{(1;\Delta x)}(v\partial_y u)_{jk} \big] (x_{i+1/2}) + O(\Delta x^{2s-1}, \Delta y^{2s}) \end{aligned} \tag{17d}$$

where by [24, (8b), p. 2767] $O(\Delta x^{2s})$ accuracy is recovered, in (17d) for the particular value $\xi = \frac{1}{2}$. Finally

$$\frac{\left[\check{F}_{(v\partial_y u),\mathrm{S}\begin{pmatrix} i,s-1,s \\ j,s\ \ ,s \\ k,0\ \ ,0 \end{pmatrix}} \right]_{i+\frac{1}{2},j,k} - \left[\check{F}_{(v\partial_y u),\mathrm{S}\begin{pmatrix} i-1,s-1,s \\ j\ \ ,s\ \ ,s \\ k\ \ ,0\ \ ,0 \end{pmatrix}} \right]_{i-\frac{1}{2},j,k}}{\Delta x} = \frac{\partial}{\partial x} \left(v \frac{\partial u}{\partial y} \right) \Big|_{ijk} + O(\Delta x^{2s}, \Delta y^{2s}) \tag{17e}$$

Similar relations apply for the different cross-derivatives appearing in (16b, 16d). At near-boundary points, we use biased stencils, in analogy with (§2.7).

3.3 Accuracy test

To check that the application of the proposed scheme for the line-derivatives (§2.4), coupled with the usual approach for the cross-derivatives (§3.2), returns the theoritical order-of-accuracy numerical results for $\mathrm{div}\boldsymbol{\tau}$ (16b) and $\mathrm{div}\left(\vec{V}.\boldsymbol{\tau} - \vec{q}\right)$ (16d) corresponding to the hypothetical field

$$\begin{aligned} u(x,y,z) &:= \sin 4\pi x\ \sin 2\pi y\ \sin 3\pi z \\ v(x,y,z) &:= \sin 5\pi x\ \sin 4\pi y\ \sin 3\pi z \\ w(x,y,z) &:= \sin 5\pi x\ \sin 3\pi y\ \sin 7\pi z \\ T(x,y,z) &:= \sin 6\pi x\ \sin 8\pi y\ \sin 9\pi z + 2 \\ \mu(x,y,z) &:= e^{xyz} \\ \lambda(x,y,z) &:= e^{xyz} \\ \mu_{\mathrm{B}} &:= 0 \end{aligned} \tag{18}$$

are compared (Fig. 6) with the analytical solution obtained by straightforward differenciation in (16b, 16d).

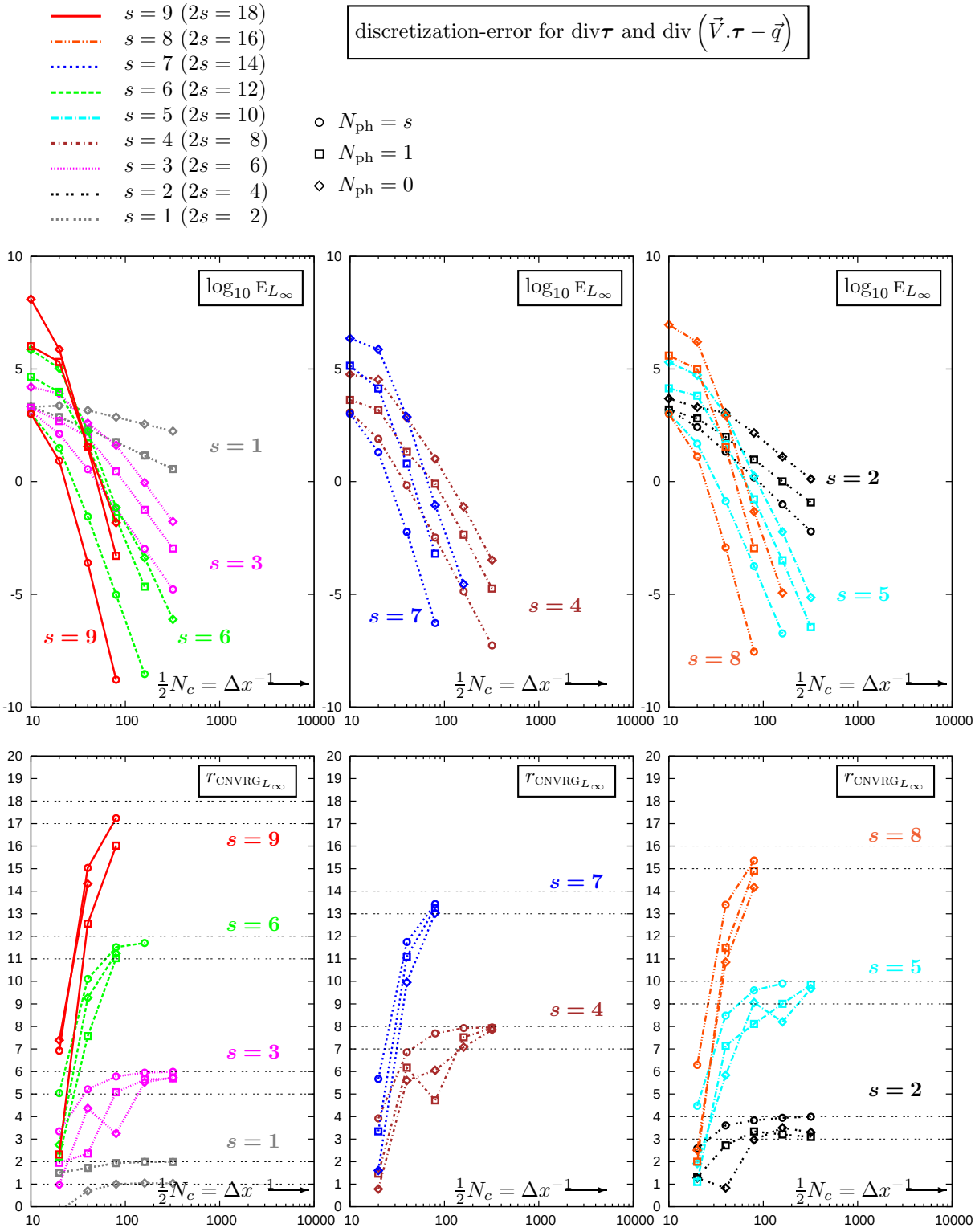

Figure 6: L_∞-norm error E_{L_∞} (19) and rate-of-convergence $r_{\mathrm{CNVRG}_{L_\infty}}$ (8b), as a function of the number of grid-cells $N_c = N_i - 1 = N_j - 1 = N_k - 1$, of the numerical approximation of div$\boldsymbol{\tau}$ and div$\boldsymbol{\tau}$ by the present method (6, 9) with $s \in \{1, \cdots, 9\}$, for the test-case (18), using $N_{\rm ph} \in \{0, 1, s\}$ phantom nodes on progressively refined computational grids ($N_i = 21, 41, 81, 161, 321$ points depending on the value of the order-parameter s).

The fields (18) and the coordinates (x, y, z) are assumed to be nondimensional quantities, so that the norm (19) is used.

$$E_{L_\infty}(N_c) := \max_{i,j,k} \left\{ \begin{array}{l} \Big| [(\mathrm{div}\boldsymbol{\tau})_x]_{\mathrm{num}} - [(\mathrm{div}\boldsymbol{\tau})_x]_{\mathrm{exact}} \Big|, \\ \Big| [(\mathrm{div}\boldsymbol{\tau})_y]_{\mathrm{num}} - [(\mathrm{div}\boldsymbol{\tau})_y]_{\mathrm{exact}} \Big|, \\ \Big| [(\mathrm{div}\boldsymbol{\tau})_z]_{\mathrm{num}} - [(\mathrm{div}\boldsymbol{\tau})_z]_{\mathrm{exact}} \Big|, \\ \Big| [\mathrm{div}(\vec{V}\cdot\boldsymbol{\tau}) - \vec{q}]_{\mathrm{num}} - [\mathrm{div}(\vec{V}\cdot\boldsymbol{\tau} - \vec{q})]_{\mathrm{exact}} \Big| \end{array} \right\} \quad ; \quad i,j,k \in \{1,\cdots,N_c+1\} \tag{19}$$

4 Conclusions

The present work defines numerical fluxes for very-high-order finite-volume conservative discretization of $(\mu u')$, applicable to the viscous terms of the Navier-Stokes equations. Future work includes the development of WENO discretizations of these terms for flows with discontinuities.

The present scheme is almost twice more accurate on a given stencil $\mathrm{S}_{i,s,s}$ than previous approaches [14, 17] based on finite differencing (equivalently yields the same accuracy as previous approaches on almost twice more compact, for large s, stencils). It is also conceptually simpler, in that it simply uses polynomial interpolation and reconstruction on the entire stencil in lieu of 2 levels of finite differencing on substencils.

The extension of the method to unstructured finite-volume meshes is straightforward, by using edge-based reconstruction.

Acknowledgments

Computer resources were made available by IDRIS–CNRS (www.idris.fr). The authors are listed alphabetically.

All the computer programs developed and used in the present work are open source and can be found at http://aerodynamics.sourceforge.net. The package includes all the reconstruction routines (in f90 language), and their application to the various test-cases.

References

[1] N. A. Adams and K. Shariff. A high-resolution hybrid compact-ENO scheme for shock/turbulence interaction problems. *J. Comp. Phys.*, 127:27–51, 1996.

[2] J. Sesterhenn. A characteristic-type formulation of the Navier-Stokes equations for high-order upwind schemes. *Comp. Fluids*, 30:37–67, 2001.

[3] N. D. Sandham, Q. Li, and H. C. Yee. Entropy splitting for high-order numerical simulation of compressible turbulence. *J. Comp. Phys.*, 178:307–322, 2002.

[4] S. Pirozzoli. Conservative hybrid compact-WENO schemes for shock-turbulence interaction. *J. Comp. Phys.*, 178:81–117, 2002.

[5] D. Ponziani, S. Pirozzoli, and F. Grasso. Development of optimized WENO schemes for multiscale compressible flows. *Int. J. Num. Meth. Fluids*, 42:953–977, 2003.

[6] M. P. Martín, E. M. Taylor, M. Wu, and V. G. Weirs. A bandwidth-optimized WENO scheme for effective direct numerical simulation of compressible turbulence. *J. Comp. Phys.*, 220:270–289, 2006.

[7] E. M. Taylor, M. Wu, and M. P. Martín. Optimization of nonlinear error for weighted essentially non-oscillatory methods in direct numerical simulations of compressible turbulence. *J. Comp. Phys.*, 223:384–397, 2007.

[8] G. A. Gerolymos, D. Sénéchal, and I. Vallet. Performance of very-high-order upwind schemes for DNS of compressible wall-turbulence. *Int. J. Num. Meth. Fluids*, 63:769–810, July 2010.

[9] C. W. Shu. High-order WENO schemes for convection-dominated problems. *SIAM Rev.*, 51(1):82–126, February 2009.
[10] S. K. Lele. Compact finite difference schemes with spectral-like resolution. *J. Comp. Phys.*, 103:16–42, 1992.
[11] M. R. Petersen and D. Livescu. Forcing for statistically stationary compressible isotropic turbulence. *Phys. Fluids*, 22:116101(1–11), 2011.
[12] G. A. Gerolymos, D. Sénéchal, and I. Vallet. Very-high-order WENO schemes. *J. Comp. Phys.*, 228:8481–8524, December 2009.
[13] M. Vinokur. An analysis of finite-difference and finite-volume formulations of conservation laws. *J. Comp. Phys.*, 81:1–52, 1989.
[14] D. W. Zingg, S. DeRango, M. Nemec, and T. H. Pulliam. Comparison of several spatial discretizations for the Navier-Stokes equations. *J. Comp. Phys.*, 160:683–704, 2000.
[15] G. S. Jiang and C. W. Shu. Efficient implementation of weighted ENO schemes. *J. Comp. Phys.*, 126:202–228, 1996.
[16] D. S. Balsara and C. W. Shu. Monotonicity prserving WENO schemes with increasingly high-order of accuracy. *J. Comp. Phys.*, 160:405–452, 2000.
[17] Y. Q. Shen, G. C. Zha, and X. Chen. High-order conservative differencing for viscous terms and the application to vortex-induced vibration flows. *J. Comp. Phys.*, 228:8283–8300, 2009.
[18] G. Gassner, F. Lörcher, and C. D. Munz. A contribution to the construction of diffusion fluxes for finite-volume and discontinuous galerkin schemes. *J. Comp. Phys.*, 224:1049–1063, 2007.
[19] M. Ben-Artzi and J. Falcovitz. *Elementary Numerical Analysis*. Cambridge University Press, Cambridge [GBR], 2003.
[20] G. A. Gerolymos. A general recurrence relation for the weight-functions in Mühlbach-Neville-Aitken representations with application to WENO interpolation. *ArXiv*, 2011:1102.1826(1–7), February 2011. (http://arxiv.org/pdf/1102.1826; submitted to *Appl. Math. Comp.*, 16 feb 2011).
[21] G. A. Gerolymos. Approximation error of the Lagrange reconstructing polynomial. *J. Approx. Theory*, 163(2):267–305, February 2011.
[22] C. W. Shu. ENO and WENO schemes for hyperbolic conservation laws. In A. Quarteroni, editor, *Advanced Numerical Approximation of Nonlinear Hyperbolic Equations, by B. Cockburn, C. Johnson, C. W. Shu and E. Tadmor*, volume 1697 of *Lecture Notes in Mathematics*, chapter 4, pages 325–432. Springer, Berlin [DEU], 1998. (also NASA CR–97–206253 and ICASE–97–65 Rep., NASA Langley Research Center, Hampton [VA, USA]).
[23] P. Henrici. *Elements of Numerical Analysis*. John Wiley and Sons, New York [NY, USA], 1964.
[24] G. A. Gerolymos. Representation of the Lagrange reconstructing polynomial by combination of substencils. *J. Comp. Appl. Math.*, 236:2763–2794, 2012.
[25] G. A. Gerolymos. reconstruction.mac (a maxima package for the analysis of reconstruction-based computational schemes). http://aerodynamics.fr/maxima, 2009.
[26] S. D. Conte and C. de Boor. *Elementary Numerical Analysis*. McGraw-Hill, New York [NY, USA], 1980.
[27] M. F. White. *Viscous Fluid Flow*. McGraw-Hill, New York [NY, USA], 1974.
[28] G. A. Gerolymos. Implicit multiple-grid solution of the compressible Navier-Stokes equations using k$-\varepsilon$ turbulence closure. *AIAA J.*, 28(10):1707–1717, October 1990.
[29] H. Lomax, T. H. Pulliam, and D. W. Zingg. *Fundamentals of Computational Fluid Dynamics*. Springer, Berlin [DEU], 1. (corrected 2. printing 2003) edition, 2001.
[30] G. A. Gerolymos and I. Vallet. Implicit mean-flow-multigrid algorithms for Reynolds-stress-model computations of 3-D anisotropy-driven and compressible flows. *Int. J. Num. Meth. Fluids*, 61(2):185–219, September 2009.